

INSTABILITY IN VISCOELASTIC THIN FILMS

A Thesis submitted

In Partial Fulfillment of the Requirements

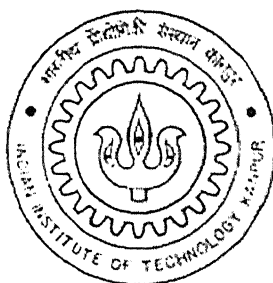
For the Degree of

Master of Technology

by

SACHIN KUMAR SHUKLA

Roll No : Y3102030



to the

DEPARTMENT OF CHEMICAL ENGINEERING
INDIAN INSTITUTE OF TECHNOLOGY, KANPUR

June, 2005

TH
CHE/2005/M
Sh 02 i

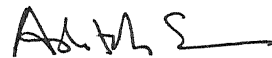
12 SEP 2005/CHE
दुखोत्तम काशीनाथ केलकर पुस्तकालय
भारतीय प्रौद्योगिकी संस्थान कानपुर
बप्रापि क्र० A...152784



A152784

CERTIFICATE

It is certified that the work contained in the thesis entitled “Instability in viscoelastic thin films” by Sachin Kumar Shukla, has been carried out under my supervision and that this work has not been submitted elsewhere for a degree.



Prof. Ashutosh Sharma

Department of Chemical Engineering

I. I. T. Kanpur

June 2005



Dedicated to

My Parents & My Brother

ACKNOWLEDGEMENTS

I would like to express my deep gratitude to my guide, Prof. **Ashutosh Sharma**. A gem of person a great researcher, his motivational words and valuable suggestions always enlightened my thought and made the work progress in a smooth manner. The opportunity to work with him was one of the most fortunate parts of my learning. His smart talks to the problem always inspired me in search of the solution. His role in fostering an inquisitive spirit in search of solution played a big role in developing in me deep interest for research.

I would like to express my indebtedness to Dr. **V. Shankar**, who not only modeled the equations for me but also helped me in solving them.

This thesis would not have been possible without **Baba** (Gaurav). The nights of computations with him, his constant advices and friendly scoldings always kept me on my toes to finish the job in time.

Dipankar, Ruhi, Jayati and Ritesh were perfect lab mates, I am very much thankful for their participations in the discussion and bringing an enthusiasm in the talks. I would like to express my thanks to **Rajeev**, he not only regarded me as a younger brother but was always a friendly mentor and “guide” who constantly “guided” me and taught me the intricacies of life and relationships and gave valuable insights regarding human nature. Again I would like to thank **Bhupesh (Bhupi)**, my astrologer friend, for teaching me how to smile and laugh even in the toughest times and for showing me the vast and hitherto uncharted domains of life.

The days at IITK can't be measured; the lifetime assets **Satish, Manjhi, Ravi, Praveen, Ethaya, Kasturi, Satyam, Subbu** and **Sonny** have been treasured in my heart. I would like to add my B.Tech batch mates **Mansoor, Veeresh, Amit, Jajoo, Piyush, Mayank, Priyam and Pranjal** for unforgettable togetherness at IITK.

No words could express my deepest gratitude for my lovable **parents** and brother, **Basu**; for always being by my side whenever I needed them. This thesis would have certainly not been possible without their prayers and well-wishes. Last but not the least I would like to acknowledge my wonderful appreciation of **Riya** for always being with me.

Sachin Kumar Shukla

ABSTRACT

Evolution of thin viscoelastic liquid films has been studied using Oldroyd-B model for stress-strain rate constitutive relationship and the simplifying the Governing differential equation under lubrication approximation. 2-D Numerical simulations have been performed of the nondimensionalized equations. Presence of a polymer in a Newtonian solvent makes the solution viscoelastic. Instead of being linear, long polymer chains try to bring each other to randomize the system and hence increase the entropy, which shows the elastic behavior of viscoelastic fluids. It was found that the length scale of instability is not affected by the inclusion of elasticity in the liquid, which is due to the presence of polymer in the solution. But time scale of instability is much affected and is very sensitive to the elasticity of fluid especially in Maxwell model when only polymer is present in the solution. As the elasticity of solution is increased there is a decrease in the time scale, which shows the destabilizing effect of elasticity. As the film surface touches the substrate and starts forming a hole, a rim around the hole forms and rim height increases linearly with the hole diameter. Effect of bending moment in the Newtonian fluid is also considered. Bending moment, like the surface tension, has a stabilizing effect. 3D simulations are also carried to show how the pattern changes with the height.

TABLE OF CONTENT

1 Introduction

1.1	Thin films.....	1
1.2	Literature Review.....	2
1.3	Outline of present study.....	3

2 Instability in viscoelastic thin films

2.1	Theory.....	4
2.2	Constitutive equation.....	5
2.3	System of Study.....	6
2.4	Free energy of thin films.....	7
2.5	Conservation laws.....	8
2.5.1	Mass conservation.....	9
2.5.2	Momentum conservation.....	9
2.5.3	Boundary conditions.....	9
2.6	Scaling.....	10
2.7	Linear stability analysis.....	14
2.8	Numerical method.....	16
2.9	Results and discussions.....	19
2.9.1	Random perturbation.....	19
2.9.2	Sinusoidal perturbation.....	21
2.9.3	Effect of weissenburg number on rupture time... ..	27
2.9.4	Maxwell model.....	31
2.9.5	Purely Newtonian case.....	33

2.10	Conclusions and recommendations.....	35
3	Effect of Bending moment in a cell membrane	
3.1	Introduction.....	35
3.2	Concept of bending moment.....	35
3.3	Problem formulation.....	36
3.4	Non-demensionalization.....	37
3.5	Three dimensional thin film equation.....	39
3.6	Linear stability analysis.....	39
3.7	Numerical method (2D).....	42
3.8	Numerical method (3D).....	43
3.9	Results and discussion.....	44
3.10	Conclusions and discussion.....	58
4	References.....	59

LIST OF FIGURES

2.1	Mechanistic equivalent of Oldroyd B model.....	5
2.2	Schematic diagram of a 2-D thin film on substrate.....	7
2.3	Qualitative variation of change in free energy ΔG and second derivative of change in free energy $\frac{\partial^2 G}{\partial H^2}$, with the film thickness for a type I thin film.....	8
2.4	Various stages of evolution of instability in an initially uniform film thickness of $(h_0 = 6.85)$ nm. And weissenberg number $(w = 4.0)$, on a length scale of 3Λ	20
2.5	Full morphology starting with a sinusoidal perturbation in a viscoelastic film of initial thickness $h_0 = 6.85$ and $(\eta_r = 0.5, w = 4.0)$ over a length scale of 2Λ	22
2.6	Variation of maximum growth coefficient as a function of weissenberg number, η_r as the parameter.....	23
2.7	The deviation of amplitude increases as the time increase. The dotted line shows the logarithm of amplitude $(1 - H_{\min})$ from non-linear simulation and solid straight line is the same but from linear stability analysis, for $(\eta_r = 0.5, w = 2.0)$	25
2.8	Variation between the maximum value of (I), which is volume flux passing per unit width of the film, for $(\eta_r = 0.5, w = 2.0)$. Solid line corresponds to the linear theory while dotted line corresponds to the non-linear simulation	26
2.9	Variation between the maximum value of (v), which is the surface velocity of the thin film, for $(\eta_r = 0.5, w = 2.0)$. Solid line corresponds to the linear theory while dotted line corresponds to the non-linear simulation.....	27

2.10	Variation of amplitude as a function of time, with weissenberg number as a parameter. As the value of weissenberg number increases the amplitude of instability increases and hence the rupture time decreases.....	28
2.11	Variation between rim height as hole diameter for $(\eta_r = 0.5, w = 4.0)$	29
2.12	hole diameter as a function of time, for $(\eta_r = 0.5, w = 4.0)$	30
2.13	Variation of amplitude $(1 - h_{\min})$ with respect to time, for different values of weissenberg number, for very less value of η_r , $(\eta_r = 0.01)$, and comparison with the LSA. Lines are from Linear Stability Analysis and points show the results from non-linear simulation.....	32
3.1	Configuration of system.....	37
3.2	Variation of growth coefficient with the bending moment.....	46
3.3	Variation of ϕ_h with the mean film thickness for Type IV systems. S^{LW} is 2.0 mJ/m^2 and S^{AB} is -33.0 mJ/m^2	49
3.4	Variation of ϕ_h with the mean film thickness for Type IV systems. $S^{LW} = -4.0 \text{ mJ/m}^2$ and $S^{AB} = 25.0 \text{ mJ/m}^2$	49
3.5	Final profile of the thin film, with mean height as the parameter, starting with sinusoidal perturbation, for apolar substrate, $S^{LW} = 2.0 \text{ mJ/m}^2$ and $S^{AB} = -33.0 \text{ mJ/m}^2$. Surface tension $\gamma = 0.001 \text{ mJ/m}^2$	51
3.6	Final profile of the thin film, with surface tension as the parameter, starting with sinusoidal perturbation, for apolar substrate, $S^{LW} = 2.0 \text{ mJ/m}^2$ and $S^{AB} = -33.0 \text{ mJ/m}^2$. Mean height $h_0 = 5 \text{ nm}$	52

3.7	Full morphology of thin film starting with mean film thickness $h_0 = 5$ nm. On 2Λ length scale, for apolar substrate $S^{LW} = 2.0$ mJ/m ² , $S^{AB} = -33.0$ mJ/m ² . Surface tension $\gamma = 0.001$ mJ/m ²	53
3.8	Morphology of thin film starting with mean film thickness $h_0 = 5$ nm and with random perturbation of $\varepsilon = 0.01$. On 3Λ length scale, for apolar substrate $S^{LW} = 2.0$ mJ/m ² , $S^{AB} = -33.0$ mJ/m ² . Surface tension $\gamma = 0.001$ mJ/m ²	53
3.9	Profiles of thin films on an apolar substrate, varying mean height as the parameter. $S^{LW} = -4.0$ mJ/m ² and $S^{AB} = 25.0$ mJ/m ²	54
3.10	Different stages of evolution in 5.0 nm thick film, starting with random perturbation, $l_0 = 0.6$ nm, $SLW = 2$ mJ/m ² and $S^{AB} = -33.0$ mJ/m ²	56
3.11	Different stages of evolution in 80 nm thick film, starting with random perturbation, $l_0 = 1.0$ nm, $SLW = -4$ mJ/m ² and $S^{AB} = 25.0$ mJ/m ²	57
3.12	Different stages of evolution in 3.5 nm thick film, starting with random perturbation, $l_0 = 2.5$ nm, $SLW = 4$ mJ/m ² and $S^{AB} = -0.1$ mJ/m ²	58

NOMENCLATURE

A	effective hamaker constant
B	positive constant in Born-Repulsion term
d_0	cut-off distance
G	free energy
G_1	spring constant in the visco-elastic model
h	dimensional film thickness
k	wave number of perturbation
k_c	critical wave number of perturbation
k_m	dominant wave number of perturbation
k_{my}	critical wave number of perturbation considering interfacial tension only
k_{mB}	critical wave number of perturbation considering bending moment only
l_0	cut-off distance where excess free energy is minimum
M	bending moment
p	film pressure
R_1, R_2	principal radii of curvature
s	growth coefficient
S^{LW}	LW component spreading coefficient
S^{AB}	AB component spreading coefficient
t	dimensional time
x	dimeansional space coordinate
ε	amplitude of perturbation

γ	interfacial tension
I	volume flux in the fluid film per unit depth of film
η_p	viscosity of polymer
η_s	viscosity of solvent
η_r	viscosity ratio of solvent viscosity to the total viscosity
η	sum of solvent and polymer viscosity
ϕ	dimensional potential due to intermolecular attraction
ρ	density of fluid film
Π	total pressure comprises intermolecular forces and pressure due to surface tension
w	weissenberg number
τ	stress on the fluid film
$v_{x,l}$	x component of fluid velocity at the surface

CHAPTER 1

INTRODUCTION

1.1 Thin Films

In thin films the thermodynamic and transport properties depend on the film thickness, which is less than the effective range of intermolecular interactions (usually < 100 nm). Thin films have much importance not only in scientific interests but also in the industries. Stability, morphology, adhesion failure, and defect formation in thin films are of main scientific interest in the areas like coating, painting, adhesives, floatation, multilayer adsorption etc. Thin films are widely used, for example, to provide insulating layers between conductors, diffusion barriers, and hardness coatings for scratch and wear resistance. Excess intermolecular interaction, which is the characteristic of thin films, is the main cause of the thin film instability. Excess molecular interaction is the sum of many possible components, the most important of which are Lifshitz-van der Waals forces (LW), electrostatic (EL) interactions, polar “acid-base” (AB) interactions and the extremely short range Born Repulsion (BR). Depending on the combination of these force fields, the thin films are characterized to four types of films namely, Type I, Type II, Type III, Type IV. The force fields in Type I, Type II, Type III and Type IV films are of purely attractive, long range attraction-short range repulsion, purely repulsive and long range repulsion-short range attraction respectively.

1.2 Literature Review

Instability of liquid thin films has been studied extensively and systematically for more than 40 years. Many possible pathways have been proposed and demonstrated for the transition from the initially flat and smooth film to the final state consisting of droplets. The free surface of an initially uniform thin film becomes unstable and deforms spontaneously to engender a microstructure when the second derivative of the excess intermolecular free energy (per unit area) with respect to the local film thickness is negative, viz., $\partial^2 G / \partial h^2 < 0$ [1-5]. Investigation of opening of holes in thin films, deposited onto silicon wafer coated with a polydimethylsiloxane monolayer, shows strong deviation from the behavior of pure Newtonian liquid. The highly asymmetric rim grows which varies with the diameter, linearly [11]. Polymer melts, which are Non-Newtonian in nature, do not obey linear relationship between shear stress and strain rate. Many models have been proposed to model the constitutive relationship between stress and strain of such fluids, namely, Maxwell fluid model, Voigt solid model and Oldroyd-B model. Oldroyd-B model is most general and linear viscoelasticity is considered here. The length scale of instability, in Non-Newtonian fluids, is unaffected of viscoelastic behavior of the fluid and it remains same as in the Newtonian fluids. Viscoelasticity does not determine the competition between the capillarity and intermolecular potential that set the scale for a viscous fluid while the time scale is decreased.

S. A. Safran and J. Klein [12] state that the surface of liquid thin films can be unstable due to thinning van der Waals interactions, leading to the formation of holes in the initially uniform film. These instabilities can be greatly retarded in viscoelastic materials and completely inhibited in the elastic materials.

A. Sharma *et al* [6] have shown the formation and growth of holes in apolar non-slipping Newtonian thin films subject to long-range Lifshitz-van der Waals forces are investigated based directly on numerical solutions of the thin-film. The present study is an extension of this work, where the fluid is considered to be Non-Newtonian in nature.

1.3 Outline of the present study

The chapter 2 deals with the instability in viscoelastic thin films on a homogeneous substrate. Figure 2.1 shows the viscoelastic fluid on a substrate, bounded by a bounding media like air. Some examples of viscoelastic fluids include toothpaste, soft serve ice cream, ketchup, melted chocolate and tar. We start with the theory of viscoelastic fluids, Oldroyd B model, and then constitutive equation is derived. Then for this 2-D system, Navier Stokes equation is applied, with the appropriate boundary conditions, which is scaled using the long wave approximation. The instability of the liquid film is studied, resulting, evolution of the free surface as a function of time and is compared with the linear theory. The length scale and the time scale of instability are also compared with the Newtonian case.

Chapter 3 deals with the Newtonian fluid on a solid substrate bounded by the cell membrane. The effect of bending moment on the cell membrane is studied and its effect on the length-scale and time-scale with the change in intensity of bending moment has been shown. 3-D simulation performed also show the variation in patterns with variation of the mean height of the film.

CHAPTER 2

INSTABILITY IN VISCOELASTIC THIN FILMS

2.1 Theory

Oldroyd B model is one of the many models, to understand the behavior of viscoelastic fluids, which has both the viscous property of liquid and elastic property of solid. In the Newtonian solvent, which has low molecular weight, the polymer is present which makes the solution to be viscoelastic. polymers are long, randomly arranged chains so that it can be considered as two balls connected by an elastic spring. To understand the elastic property of a polymer in the solution, we can think of long polymer chains in the solution to be randomly arranged, due to entropy constraints and have a tendency to pull back to make the process more random, and hence, increase the entropy. While doing so, the viscous behavior of the solution and polymer makes the process slow.



Figure 2.1: shows the mechanistic equivalent of Oldroyd B model, Spring shows the elastic property of polymer with spring constant G_1 .

2.2 Constitutive equation

In a Newtonian liquid, stress τ is proportional to the strain rate $\dot{\xi}$, i.e. to the gradient of the velocity field $\dot{\xi}_{ij} = \partial_i V_j + \partial_j V_i$, but in a linear elastic medium the stress is proportional to the strain ξ , but not the strain rate. The total displacement ξ in the Oldroyd B model is the sum of displacement due to polymer and Newtonian solvent ξ_p and ξ_s respectively. Stress in spring is proportional to strain while in dashpot, it is proportional to strain rate. Hence total stress can be written as the summation of these two forces.

$$\tilde{\tau} = G_1 \xi_s + \eta_s \left(\frac{\partial \xi_s}{\partial t} \right) \quad (2.1)$$

Similarly, stress in the polymeric dashpot can be written as,

$$\tilde{\tau} = \eta_p \left(\frac{\partial \xi_p}{\partial t} \right) \quad (2.2)$$

The total displacement is the sum of these two displacements.

$$\xi = \xi_s + \xi_p \quad (2.3)$$

the constitutive equation for the Oldroyd B model is given by

$$\lambda \frac{\partial \tilde{\tau}_{xy}}{\partial t} + \tilde{\tau}_{xy} = \eta \left[\lambda \eta_r \frac{\partial}{\partial t} \left(\frac{\partial V_x}{\partial y} \right) + \frac{\partial V_x}{\partial y} \right] \quad (2.4)$$

Where, x is the direction parallel to the film surface and y is the normal direction to the film surface, λ is the relaxation time (the time at which forces relax to its 37 percent)[9], $\frac{\partial V_x}{\partial y}$ is strain rate ($\dot{\gamma}$) and η is the sum of viscosities of Newtonian solution and polymeric melts ($\eta = \eta_s + \eta_p$) and η_r is the ratio of solvent viscosity to the total viscosity.

2.3 System of Study

Here we consider the thin viscoelastic liquid film (<100 nm.) --polymer mixed with Newtonian solution, -- which overall makes the solution viscoelastic, bounded by a solid support (perfectly homogeneous) from below and a bounding media (air for example) from above, is the subject of the current study. The length scale parallel to the film surface is much larger than the length scale perpendicular to the film surface and hence the lubrication approximation is valid. Such a system can be better visualized with the help of Figure 2.1 which is a schematic diagram of a supported thin viscoelastic liquid film. Here we are considering only two dimensions one parallel to substrate and one normal to the substrate.

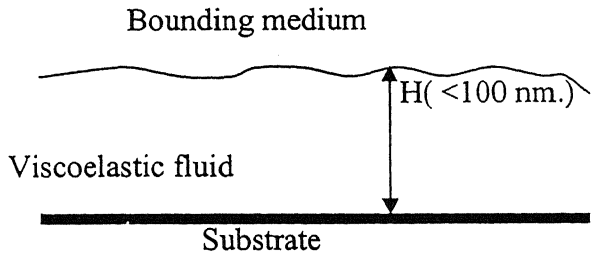


Figure 2.2 Schematic diagram of a 2-D thin film on substrate.

2.4 Free Energy of Thin Films

The equilibrium and dynamics of thin fluid films, like that of any other physical system, are related to the changes in the free energy rather than the free energy itself. Thus to understand the changes in free energy is of paramount importance to describe the mechanics of thin films. The contribution to the free energy in a system is because of interfacial tension, but if the film is less than 100 nanometer, then intermolecular forces also play an important role. Obviously the free energy change also depends on the film thickness. The disjoining pressure and excess free energy are obtained by pair wise summation of interactions among molecules of the thin film and among molecules of the film and the solid. The use of Lennard-Jones potential for intermolecular interactions gives the free energy per unit area ΔG and the conjoining pressure as the sum of their respective components due to the long-range Lifshitz-vander Waals attraction and the extremely short-range Born repulsion (5, 6, 8). Under conditions of small slope, these are

$$\Delta G = -\frac{A}{12\pi h^2} + \frac{B}{h^8} \quad (2.5)$$

And

$$\phi = \frac{A}{6\pi h^3} - \frac{8B}{h^9} \quad (2.6)$$

l_0 is the cut-off distance i.e. at which ϕ vanishes. And we know that, $A = -12\pi d_0^2 S^{LW}$, replacing these values in the above equation and using the non-dimensional parameter in equation (2.11) one can get the non dimensional equation for disjoining pressure as,

$$\Pi^0 = - \left[\frac{\partial^2 H}{\partial X^2} - \frac{1}{3H^3} \left(1 - \left(\frac{l}{H} \right)^6 \right) \right] \quad (2.7)$$

This form of potential belong to type I films where free energy change ΔG and its second derivative, $\frac{\partial^2 G}{\partial H^2}$ is negative for all film thickness.

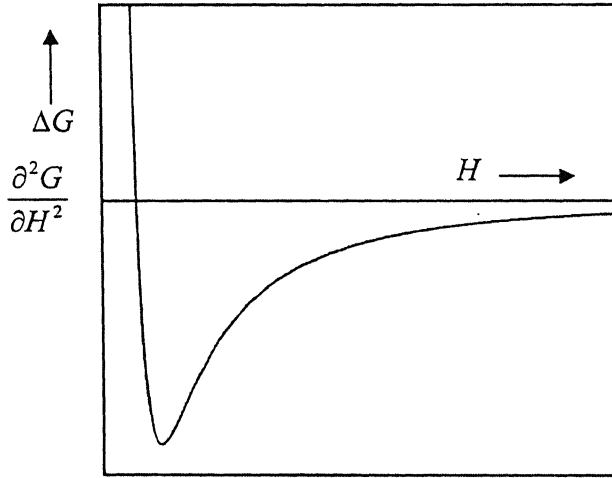


Figure 2.3. Qualitative variation of change in free energy ΔG and second derivative of change in free energy $\frac{\partial^2 G}{\partial H^2}$, with the film thickness for a type I thin film.

2.5 Conservation laws

Here we will state the hydrodynamic equations of viscoelastic fluid, and will start with the conservation laws.

2.5.1 Mass conservation

Assuming the density of fluid to be constant the equation of mass conservation reduces to

$$\nabla \cdot \mathbf{u} = 0 \quad (2.8)$$

Where \mathbf{V} is the velocity vector (V_x, V_y).

2.5.2 Momentum conservation

$$\rho \frac{d\mathbf{u}}{dt} = -\nabla \Pi + \nabla \cdot \boldsymbol{\tau} \quad (2.9)$$

Here, $\frac{d}{dt} = \partial_t + \mathbf{u} \cdot \nabla$ is the total (or material) derivative. And Π is the total pressure which comprises the pressure inside the film due to interfacial tension and the excess pressure, ϕ , which is negative of the disjoining pressure, and is related to the excess free energy per unit area of film as

$$\phi = \frac{\partial \Delta G}{\partial h} \quad (2.10)$$

The body force due to gravity is neglected compared to the body force due to excess intermolecular interactions.

2.5.3 Boundary Conditions

At the free film surface tangential component of stress is assumed to be zero and at the film-substrate interface, no slip boundary condition is assumed. Also the wall is assumed to be impermeable to the fluid, hence normal component of velocity at the substrate surface is assumed to be zero.

2.6 Scaling

The following parameters have been used for non-dimensionalizing the governing equations.

$$\begin{aligned} H &= h / h_0 & T &= t / \left(\frac{\eta h_0}{\gamma} \right) \\ V &= u / \left(\frac{\gamma}{\eta} \right) & \tau &= \tilde{\tau} / \left(\frac{\gamma}{h_0} \right) \end{aligned} \quad (2.11)$$

- h_0 is the mean film thickness
- η is the sum of both the viscosities.
- γ is the interfacial tension of liquid

Substituting these dimensional variables in terms of non-dimensional parameter in the above constitutive equation 2.4, we get the constitutive relation as

$$w_i \frac{\partial T_{xy}}{\partial T} + T_{xy} = w_i \eta_r \frac{\partial}{\partial T} \left(\frac{\partial V_x}{\partial Y} \right) + \frac{\partial V_x}{\partial Y} \quad (2.12)$$

T_{xy} is same as τ in equation (2.11) and w_i is the weissenberg constant, defined as

$$w_i = \left(\frac{\lambda \gamma}{\eta h_0} \right) \quad (2.13)$$

For very thin film the length scale of film thickness h_0 is very small than the length scale L parallel to the substrate surface. Hence, under the lubrication approximation the inertial term is not important and only the viscous term is comparable to the pressure term.

Navier Stokes momentum equation, in the x direction, under the lubrication approximation reduces to,

$$\frac{\partial \Pi}{\partial X} = \frac{\partial T_{xy}}{\partial Y} \quad (2.14)$$

and,

$$\frac{\partial \Pi}{\partial Y} = 0 \quad (2.15)$$

From the equation (2.15) we can say that, Π is function of X only. And hence equation (2.14) can be easily integrated. Integrating the equation (2.14) with respect to Y we get stress as

$$T_{xy} = \frac{\partial \Pi}{\partial X} [Y - H(X)] \quad (2.16)$$

Substituting the value of stress, obtained from equation (2.16), in the equation (2.12) we get

$$w_i \frac{\partial}{\partial T} \left[\frac{\partial \Pi}{\partial X} (Y - H(X)) \right] + \frac{\partial \Pi}{\partial X} (Y - H(X)) = \frac{\partial}{\partial Y} \left[w_i \eta_r \frac{\partial v_x}{\partial T} + v_x \right] \quad (2.17)$$

Further integrating the above equation with respect to Y we get

$$w_i \frac{\partial}{\partial T} \left[\frac{\partial \Pi}{\partial X} \left(\frac{Y^2}{2} - Y \cdot H(X, T) \right) \right] + \frac{\partial \Pi}{\partial X} \left(\frac{Y^2}{2} - Y \cdot H(X, T) \right) = w_i \eta_r \frac{\partial v_x}{\partial T} + v_x \quad (2.18)$$

Renormalizing the Π we get

$$\Pi = \varepsilon^2 \Pi^{(0)} \quad (2.19)$$

Here ε is the ratio between mean height of film and length scale.

Re-ordering the equation (2.18) we get.

$$w_i \frac{\partial}{\partial T} \left[\frac{\partial \Pi^0}{\partial X} \left(\frac{Y^2}{2} - Y \cdot H(X, T) \right) \right] + \left[\frac{\partial \Pi^0}{\partial X} \left(\frac{Y^2}{2} - Y \cdot H(X, T) \right) \right] = \eta_r w_i \frac{\partial v_{X,i}^{(0)}}{\partial T} + v_{X,i}^{(0)} \quad (2.20)$$

Further redefining the variable

$$\frac{1}{\varepsilon^4} \frac{\partial}{\partial T} = \frac{\partial}{\partial T}; \bar{w}_i = w_i \varepsilon^4 \quad (2.21)$$

Putting these redefined values in equation (2.20)

$$\bar{w}_i \frac{\partial}{\partial T} \left[\frac{\partial \Pi^0}{\partial X} \left(\frac{Y^2}{2} - Y \cdot H(X, T) \right) \right] + \left[\frac{\partial \Pi^0}{\partial X} \left(\frac{Y^2}{2} - Y \cdot H(X, T) \right) \right] = \eta_r \bar{w}_i \frac{\partial v_{X,i}^{(0)}}{\partial T} + v_{X,i}^{(0)} \quad (2.22)$$

For the 2-D flow, the kinematics equation can be written as

$$\frac{\partial H}{\partial T} + \frac{\partial}{\partial X} \int_0^{H(X,T)} dY \cdot v_{X,i}^{(0)}(Y) = 0 \quad (2.23)$$

Or

$$\frac{\partial H}{\partial T} + \frac{\partial}{\partial X} I(X, T) = 0 \quad (2.24)$$

Here I is the total flux passing per unit width of the film. Putting the value of $Y = H$ in the equation (2.22) we get the equation in interfacial velocity

$$\eta_r \bar{w}_i \frac{\partial v_{X,i}^{(0)}}{\partial T} + v_{X,i}^{(0)} = -\frac{\bar{w}_i}{2} \frac{\partial}{\partial T} \left[\frac{\partial \Pi^0}{\partial X} H^2 \right] - \frac{1}{2} \frac{\partial \Pi^0}{\partial X} H^2 \quad (2.25)$$

Here $v_{X,i}^{(0)}$ is the interfacial velocity in the x direction.

Multiplying the equation (2.22) by the dY and integrating from 0 to $H(X, T)$ and also using the Leibnitz theorem, the equation (2.22) simplifies to

$$\begin{aligned} \eta_r \bar{w}_i \frac{\partial I(X, T)}{\partial T} - \eta_r \bar{w}_i v_{x,i}^{(0)} \frac{\partial h}{\partial T} + I(X, T) = \\ - \frac{\bar{w}_i}{3} \frac{\partial}{\partial T} \left[\frac{\partial \Pi^0}{\partial X} H^3 \right] + \frac{\bar{w}_i}{2} \frac{\partial H}{\partial T} \frac{\partial \Pi^0}{\partial X} H^2 - \frac{1}{3} \frac{\partial \Pi^0}{\partial X} H^3 \end{aligned} \quad (2.26)$$

Let $\frac{\bar{w}_i}{3} = w$ and $\tilde{T} = \frac{T}{3}$ and hence $\frac{\partial}{\partial T} = \frac{1}{3} \frac{\partial}{\partial \tilde{T}}$ using these renormalized parameter in equation (2.24), (2.25), (2.26) we get 3 sets of coupled partial differential equations, which governs the instability and spatio-temporal evolution of a non-slipping viscoelastic thin liquid film subject to excess intermolecular interaction, as

$$\frac{\partial H}{\partial \tilde{T}} + 3 \frac{\partial}{\partial X} I(X, T) = 0 \quad (2.27)$$

$$3\eta_r w \frac{\partial I(X, T)}{\partial \tilde{T}} - 3\eta_r w v_{x,i} \frac{\partial H}{\partial \tilde{T}} + 3I(X, T) = -w \frac{\partial}{\partial \tilde{T}} \left[\frac{\partial \Pi^0}{\partial X} H^3 \right] + \frac{3w}{2} \frac{\partial H}{\partial \tilde{T}} \frac{\partial \Pi^0}{\partial X} H^2 - \frac{\partial \Pi^0}{\partial X} H^3 \quad (2.28)$$

$$\eta_r w \frac{\partial v_{x,i}}{\partial \tilde{T}} + v_{x,i} = -\frac{w}{2} \frac{\partial}{\partial \tilde{T}} \left[\frac{\partial \Pi^0}{\partial X} H^2 \right] - \frac{1}{2} \frac{\partial \Pi^0}{\partial X} H^2 \quad (2.29)$$

Where,

$$\frac{\partial \Pi^0}{\partial X} = -\frac{\partial}{\partial X} \left[\frac{\partial^2 H}{\partial X^2} - \frac{1}{3H^3} \left(1 - \left(\frac{l}{H} \right)^6 \right) \right] \quad (2.30)$$

The parameter used to non-dimensionalised the equation used are as follows.

$$H = \frac{h}{h_0}, X = \frac{x}{\left[h_0 (h_0 / d_0) \left(\frac{\gamma}{6(-S^{LW})} \right)^{1/2} \right]}, \tilde{T} = \frac{t}{\left[h_0 (h_0 / d_0)^4 \left(\frac{\eta\gamma}{12S^2} \right) \right]} \quad \text{and}$$

$$\Phi = \frac{\varphi}{\left[6(-S^{LW}) d_0^2 / h_0^3 \right]}$$

the Equations (2.27), (2.28) and (2.29) are the three coupled partial differential in H , I and $v_{x,l}$. Here $l = l_0 / h_0$, where l_0 is the separation distance, where excess free energy

is minimum. $\frac{\partial \Pi^0}{\partial X}$ is the derivative of disjoining pressure, the first part, second

derivative in height, shows the interfacial pressure term while the other part, which is intermolecular forces are made up of two terms, first is LW component of Vander wall forces and second is due to Born Repulsion. The viscous effect in thin films merely retards the growth of instability. The surface tension effect has stabilizing effect because of the in-plane curvature at the film surface.

- w is measure of elasticity, higher the value of w , higher the elasticity.
- η_r is the ratio of solvent viscosity to the total viscosity, if this tend to zero means we get simply the polymer solution and if it tends to 1 means we get the Newtonian solution.

2.7 Linear Stability Analysis

The initial growth of the instability in thin films can be described by linearizing the above governing equation, wherever the amplitude of the initial disturbance is much smaller

than the mean film thickness. Height is being linearized around $H=1$ and other parameter like I and v are linearized around zero (initially there is no interfacial velocity and mass flux) as:

$$H = 1 + \xi \exp(iKX + sT) \quad (2.31 \text{ a})$$

$$I = \tilde{I} \exp(iKX + sT) \quad (2.31 \text{ b})$$

$$v = \tilde{v} \exp(iKX + sT) \quad (2.31 \text{ c})$$

In the above set of equations ξ, K, T are the non-dimensional amplitude (i.e. ratio of initial disturbance amplitude and mean film thickness), wave number and growth coefficient of the initial disturbance, respectively. Linearizing the governing partial differential equation using these parameters we get a relation between non-dimensional growth coefficient and non-dimensional wave number.

$$\eta_r w s^2 + \left\{1 - w(K^2 - K^4)\right\} s - (K^2 - K^4) = 0 \quad (2.32)$$

Also, the disturbance in velocity and flux can be obtained in terms of disturbance in height and hence flux and velocity can be written as:

$$H = 1 + \xi \exp(iKX + sT) \quad (2.33 \text{ a})$$

$$I = \frac{\xi s}{3K} \exp\{i(KX + \pi/2) + sT\} \quad (2.33 \text{ b})$$

$$v = \frac{(ws + 1)\xi(K - K^3)}{2(1 + \eta_r ws)} \exp\{i(KX + \pi/2) + sT\} \quad (2.33 \text{ c})$$

The above equation which is a quadratic equation in 's', can be solved to get the linear dispersion relation, as a function of non-dimensional wave number. The critical wave number, at which growth coefficient is zero, comes out to be $K_c = 1$ i.e. only the modes

with non-dimensional wave number less than unity can grow, and the non-dimensional length scale of the fastest growing linear mode, where growth coefficient is maximum, comes out to be $2\sqrt{2}\pi$.

The maximum value of growth coefficient is:

$$s_{\max} = \frac{-4 + w + \sqrt{16 + 8(2\eta_r - 1)w + w^2}}{8\eta_r w} \quad (2.34)$$

Further more, the time of rupture (i.e. the first time at which film surface touches the solid substrate) from the linear stability analysis comes out to be:

$$T_R = \frac{1}{s_{\max}} \log_e \left(\frac{1}{\xi} \right) \quad (2.35)$$

2.8 Numerical Method

The following (2-D) set of Non-dimensional equation, governs the stability and spatio-temporal evolution of the thin film subject to the excess intermolecular interactions.

$$\frac{\partial H}{\partial \tilde{T}} + 3 \frac{\partial}{\partial X} I(X, T) = 0 \quad (2.36)$$

$$3\eta_r w \frac{\partial I(X, T)}{\partial \tilde{T}} - 3\eta_r w v_{X,I} \frac{\partial H}{\partial \tilde{T}} + 3I(X, T) = -w \frac{\partial}{\partial \tilde{T}} \left[\frac{\partial \Pi^0}{\partial X} H^3 \right] + \frac{3w}{2} \frac{\partial H}{\partial \tilde{T}} \frac{\partial \Pi^0}{\partial X} H^2 - \frac{\partial \Pi^0}{\partial X} H^3 \quad (2.37)$$

$$\eta_r w \frac{\partial v_{X,I}}{\partial \tilde{T}} + v_{X,I} = -\frac{w}{2} \frac{\partial}{\partial \tilde{T}} \left[\frac{\partial \Pi^0}{\partial X} H^2 \right] - \frac{1}{2} \frac{\partial \Pi^0}{\partial X} H^2 \quad (2.38)$$

These are coupled partial differential equations with $\frac{\partial}{\partial \tilde{T}}$ appearing in the right as well as in the left side of the equation; i.e. the above equation is not explicit in time. Because these are not explicit differential equations, hence all $\frac{\partial}{\partial \tilde{T}}$ terms are collected in one side, and $\frac{\partial H}{\partial \tilde{T}}$ is replaced by $-3\frac{\partial I}{\partial X}$ in the last two equations, to make it explicit in space.

This is fourth order in space and first order in time. We convert the above Partial differential equation into a set of ' N ' Ordinary differential equation, using the finite difference technique. These equations are discretized in space using central differential method with half node interpolation. Initial condition on height can be taken to be either sinusoidal or random perturbation; while for interfacial velocity and flux are assumed to be zero in the initial stages. Collecting the time derivative terms in one side, the equation converts to:

$$\frac{\partial H}{\partial \tilde{T}} + 3\frac{\partial}{\partial X} I(X, T) = 0 \quad (2.39)$$

$$\frac{\partial}{\partial \tilde{T}}(p_1) = -3I - 9\eta_r w v_{x,l} \frac{\partial I}{\partial X} - \frac{9w}{2} \frac{\partial I}{\partial X} \frac{\partial \Pi^0}{\partial X} H^2 - \frac{\partial \Pi^0}{\partial X} H^3 \quad (2.40)$$

$$\frac{\partial}{\partial \tilde{T}}(p_2) = -v_{x,l} - \frac{1}{2} \frac{\partial \Pi^0}{\partial X} H^2 \quad (2.41)$$

Where,

$$p_1 = 3\eta_r w I + w \frac{\partial \Pi^0}{\partial X} H^3 \quad (2.42)$$

$$p_2 = \eta_r w v_{x,l} + \frac{w}{2} \frac{\partial \Pi^0}{\partial X} H^2 \quad (2.43)$$

In the above equation the term containing the time derivative is only H , p_1 and p_2

Using the central differential technique to discretize flux in space

$$\frac{\partial H_i}{\partial \tilde{T}} = -3 \frac{\partial I_i}{\partial X} = -3 \frac{I_{i+1} - I_{i-1}}{2\Delta X} \quad (2.44)$$

$$\frac{\partial p_{1i}}{\partial \tilde{T}} = F_i \quad (2.45)$$

$$\frac{\partial p_{2i}}{\partial \tilde{T}} = G_i \quad (2.46)$$

Where

$$F_i = -3I_i - 9\eta_r w v_{x,i} \frac{\partial I_i}{\partial X} - \frac{9w}{2} \frac{\partial I_i}{\partial X} \frac{\partial \Pi_i^0}{\partial X} H_i^2 - \frac{\partial \Pi_i^0}{\partial X} H_i^3 \quad (2.47)$$

And

$$G_i = \left(-v_{x,i} - \frac{1}{2} \frac{\partial \Pi_i^0}{\partial X} H_i^2 \right) \quad (2.48)$$

In the above equation I_i and $v_{x,i}$ are given by:

$$I_i = \left(p_{1i} - w \frac{\partial \Pi_i^0}{\partial X} H_i^3 \right) / (3\eta_r w) \quad (2.49)$$

$$v_{x,i} = \left(p_{2i} - \frac{w}{2} \frac{\partial \Pi_i^0}{\partial X} H_i^2 \right) / (\eta_r w) \quad (2.50)$$

The above set of partial differential equations was solved with periodic boundary condition over an interval sufficiently large compare to $2\sqrt{2}\pi$. The initial condition was small amplitude ($\xi = 0.01$) sinusoidal or random perturbation. NAG library subroutine D02EJF, which employs the Gear's algorithm and is most suited for solving coupled, stiff ODES, was used to solve these set of ODES. 700 grid points in 2Λ scale is found to be sufficient for grid conversion test.

2.9 Results and Discussion

Like the Newtonian fluid in viscoelastic fluids also the three distinct regimes of the hole growth are identified.

1. A short, unsteady phase in which there is faster change in velocity as well as in contact angle.
2. Quasi-steady phase in which changes are very slow.
3. Finally the rims of a hole starts impeding the neighboring hole rim and form a bigger equilibrium drop.

2.9.1 Random perturbation

Figure 2.4. Shows the evolution of instability starting from nearly uniform film thickness (with a random perturbation of $(\varepsilon = 0.01)$) until the formation of a dry drop, i.e. the first time when film surface touches the substrate surface. A length scale for the simulation was chosen of 3Λ , with the initial film randomly perturbed, and in the first phase of evolution 3 waves started forming. Hence the length scale predicted by the simulation is in compliance with the length scale predicted by the linear theory. Length scale predicted by linear theory is the same as we obtained for the Newtonian case. But the time scale of instability (will be shown later) is lesser than the Newtonian case. The instability occurs because derivative of conjoining pressure with respect to height is negative, which shows higher pressure at lower thickness and vice-versa. In the beginning, if a random perturbation is given, then perturbation rearranges itself and in rearranging its amplitude decreases initially and after some time it starts growing and then ruptures, leading to rim interaction and finally droplet formation takes place.

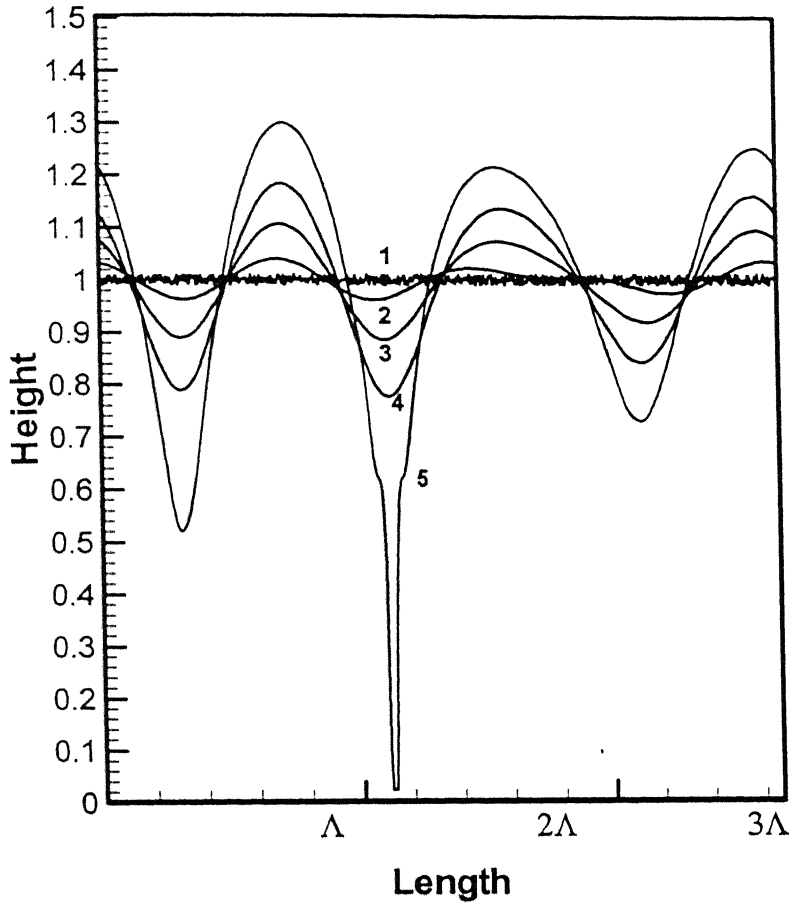


Figure 2.4. Various stages of evolution of instability in an initially uniform film thickness of $(h_0 = 6.85)$ nm. And weissenberg number $(w = 4.0)$, on a length scale of 3Λ . Curves 1-5 correspond to $T_R = 0, 12.282, 15.906, 17.307, 18.310$.

Small slope approximation is valid as long as the contact angle between liquid and solid at all stages of the hole growth is small. Visually it gives the impression that at the each stage of the hole growth, the contact angle is high but this is because we are taking larger value of X axis domain on a smaller scale in plotting, compare to the thickness scale.

2.9.2 Sinusoidal perturbation

Figure 2.5 shows the full morphology of instability in thin viscoelastic liquid films under the sinusoidal perturbation, for $\eta_r = 0.5, w = 4.0$. The wavelength of the sinusoidal perturbation is taken as the dominant wavelength and simulation is carried over the length scale of two-wave length. The evolution comes out to be symmetric i.e. both the waves start growing with the same rate, touches the surface, hole growth and its evolution all are occurring at the same time. If the simulation is carried out for the wavelength less than the critical wave length (predicted by linear theory) i.e. at which growth coefficient is negative, it was found that perturbations does not evaluate and after some time all the perturbations die out, which matches well with the linear theory. A rim forms rapidly around the expanding hole (curve 4) and grows with the expansion of the hole (curve 5 and 6 in Figure 2.5). As the rim starts to grow, it feels the effect of neighboring rims also (curve 7) which causes hindered phase of expansion. And finally merger of rims takes place and they form a bigger drop. Film evolution until rupture is slow, after rupture, the time taken to rim formation, coalition and finally forming a bigger drop is very less. Faster evolution after rupture is due to the surface tension which although initially was opposing the instability but later supports the formation of the drop, which corresponds to another more stable (meta-stable) film configuration.

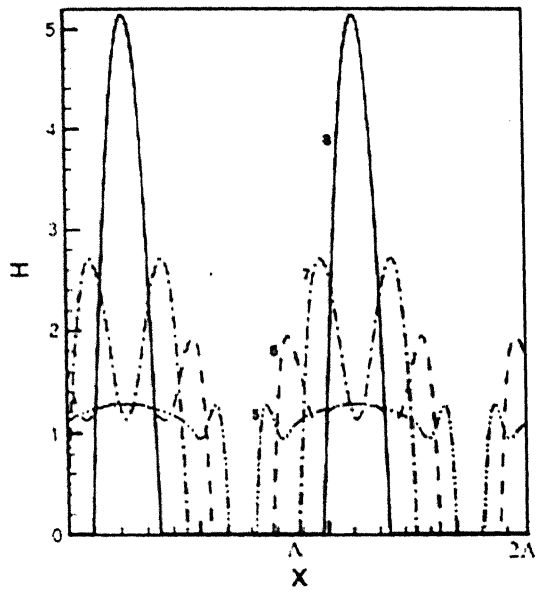
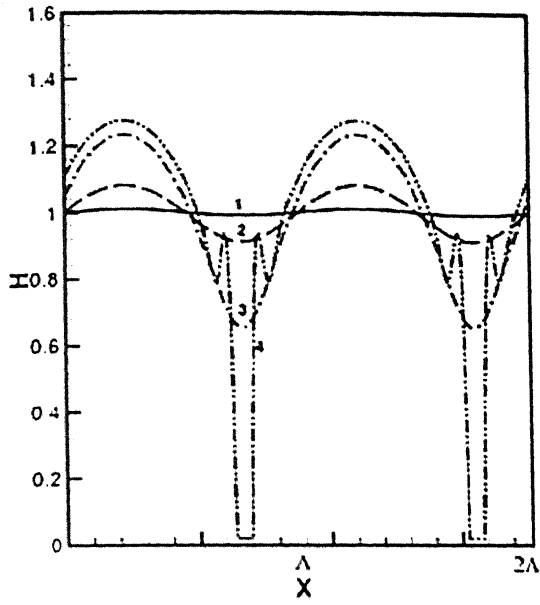


Figure 2.5. Full morphology starting with a sinusoidal perturbation in a viscoelastic film of initial thickness $h_0 = 6.85$ and $(\eta_r = 0.5, w = 4.0)$ over a length scale of 2Λ , curve 1-8 corresponds to $t_R = 0, 5.953, 8.666, 9.019, 9.021, 9.026, 9.037, 9.0482$.

Figure 2.6 shows the variation of maximum growth coefficient as a function of weissenberg number with η_r as the parameter. When $\eta_r=0$ simply we get Maxwell fluid. The variation of maximum growth coefficient as a function of weissenberg number for Maxwell case comes out to be,

$$s_{\max} = \frac{1}{4-w} \quad \text{If } w < 4 \quad (2.51)$$

And for Newtonian case ($\eta_r = 1.0$) it is independent of weissenberg number.

$$s_{\max} = \frac{1}{4} \quad \text{For Newtonian fluid} \quad (2.52)$$

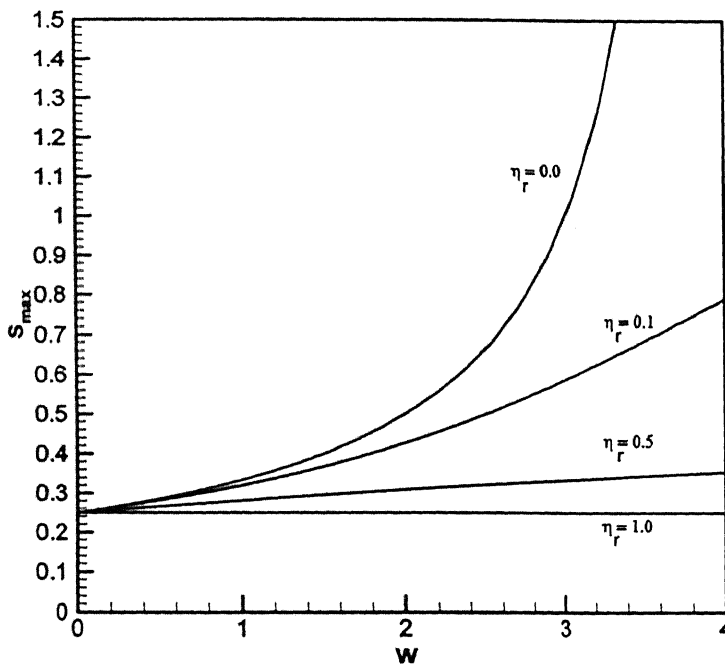


Figure 2.6. Variation of maximum growth coefficient as a function of weissenberg number, η_r as the parameter.

Some important results as predicted by linear theory are given in the following paragraph.

The dominant wavelength is proportional to $h_0^2 (-S^{LW})^{-0.5}$ which means that for thicker films and less non-wettable substrate would respond with longer dominant waves during the evolution of instability. The number density of holes is proportional to $h_0^{-4} (-S^{LW})$ which means that thinner films and more non-wettable films have higher hole

density. The minimum time of rupture is proportional to $\frac{h_0^5}{(-S^{LW})^2}$ which means that

thinner films and higher non-wettable films are prone to rupture faster. The cut-off distance and dominant wavelength predicted by linear theory are also in compliance with the nonlinear numerical solutions.

Figure 2.7 shows the amplitude as a function of time from linear theory and non-linear simulation.

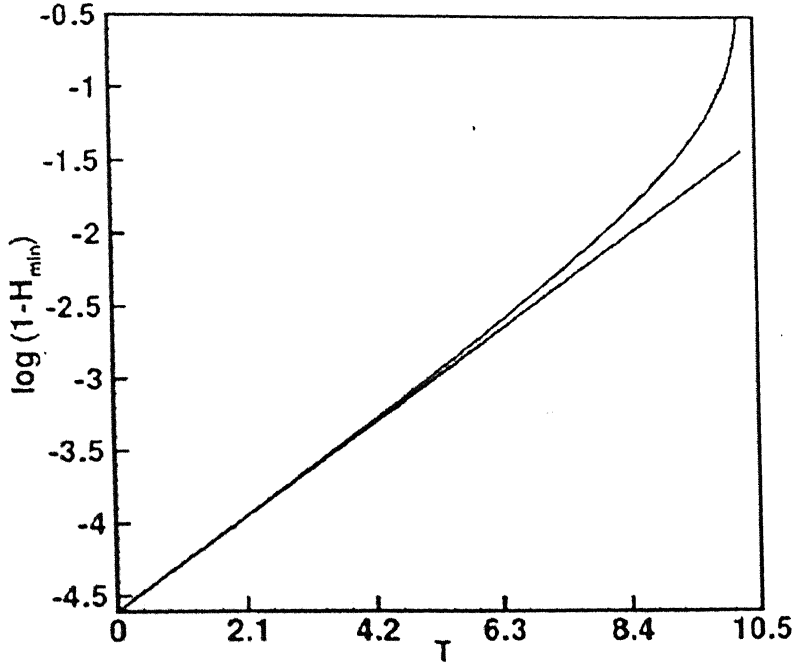


Figure 2.7. The deviation of amplitude increases as the time increase. The dotted line shows the logarithm of amplitude $(1-H_{\min})$ from non-linear simulation and solid straight line is the same but from linear stability analysis, for $(\eta_r = 0.5, w = 2.0)$.

From figure 2.7 it is clear that in the initial stages of time non-linear result of amplitude has good match with the linear theory but as the time increases the instability starts grow more rapidly than the expected value from linear theory. This is because the linear theory predicts the time of rupture according to $\left(\frac{\partial \phi}{\partial h}\right)_{h=h_0}$ i.e. according to the initial potential but as the instability grows this term decreases rapidly resulting into smaller rupture times than those predicted by the linear theory. This is the reason that as the time increases the actual non-linear amplitude deviates from the amplitude given by linear theory.

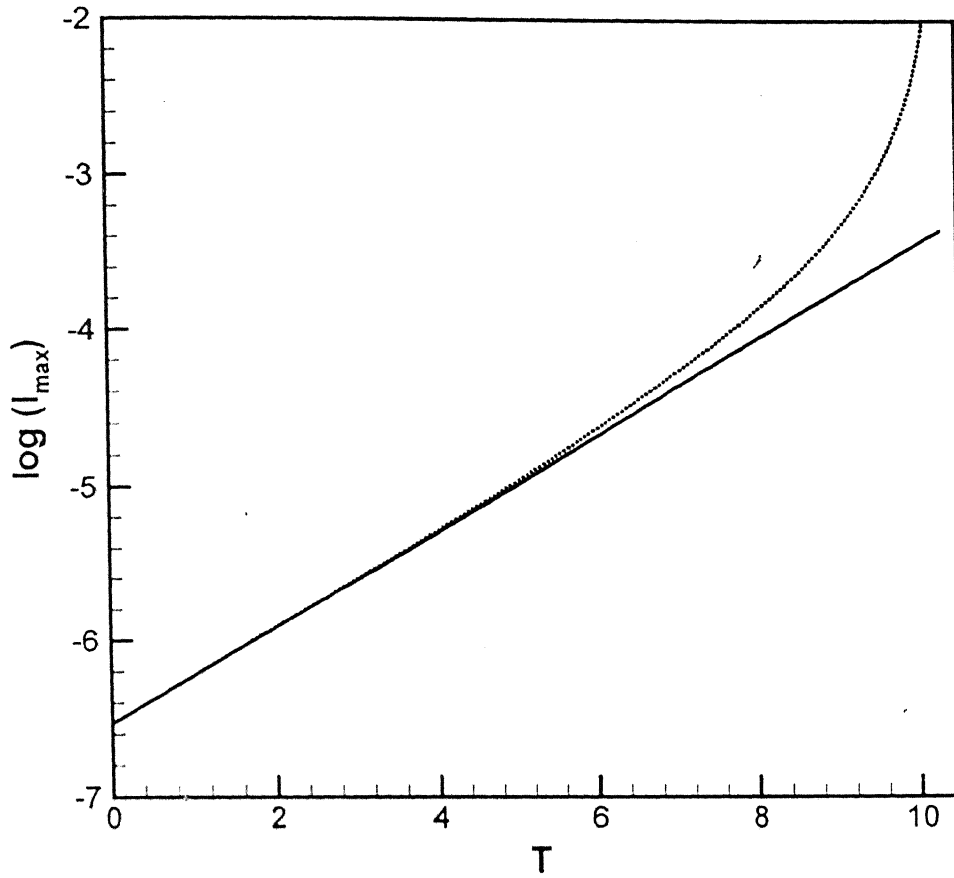


Figure 2.8 Variation between the maximum value of (I) , which is volume flux passing per unit width of the film, for $(\eta_r = 0.5, w = 2.0)$. Solid line corresponds to the linear theory while dotted line corresponds to the non-linear simulation.

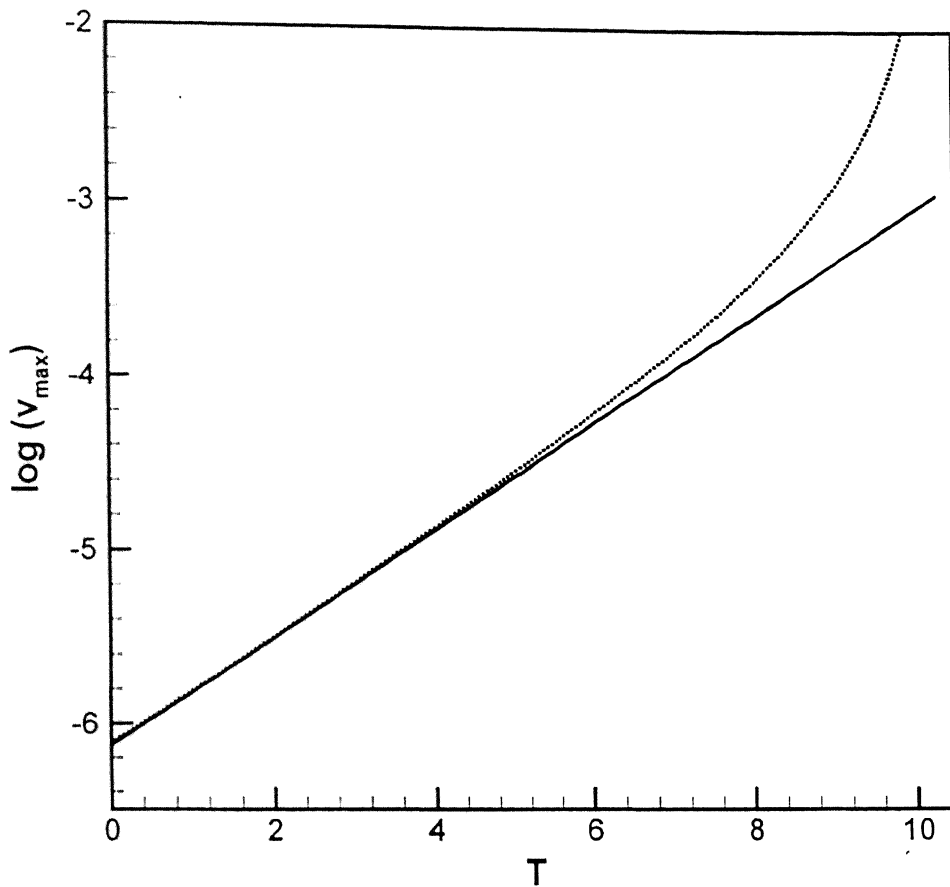


Figure 2.9. Variation between the maximum value of (v) , which is the surface velocity of the thin film, for $\eta_r = 0.5$, $w = 2.0$. Solid line corresponds to the linear theory while dotted line corresponds to the non-linear simulation.

From the above two graphs it is clear that as the time increases these values deviates from the linear stability theory.

2.9.3 Effect of weissenberg number on Rupture time

The weissenberg number has immense effect on film rupture time, in the figure below (Figure 2.10) it is clear, as the elasticity increases, i.e. weissenberg number increases, the

elasticity has destabilizing effect on the film stability.

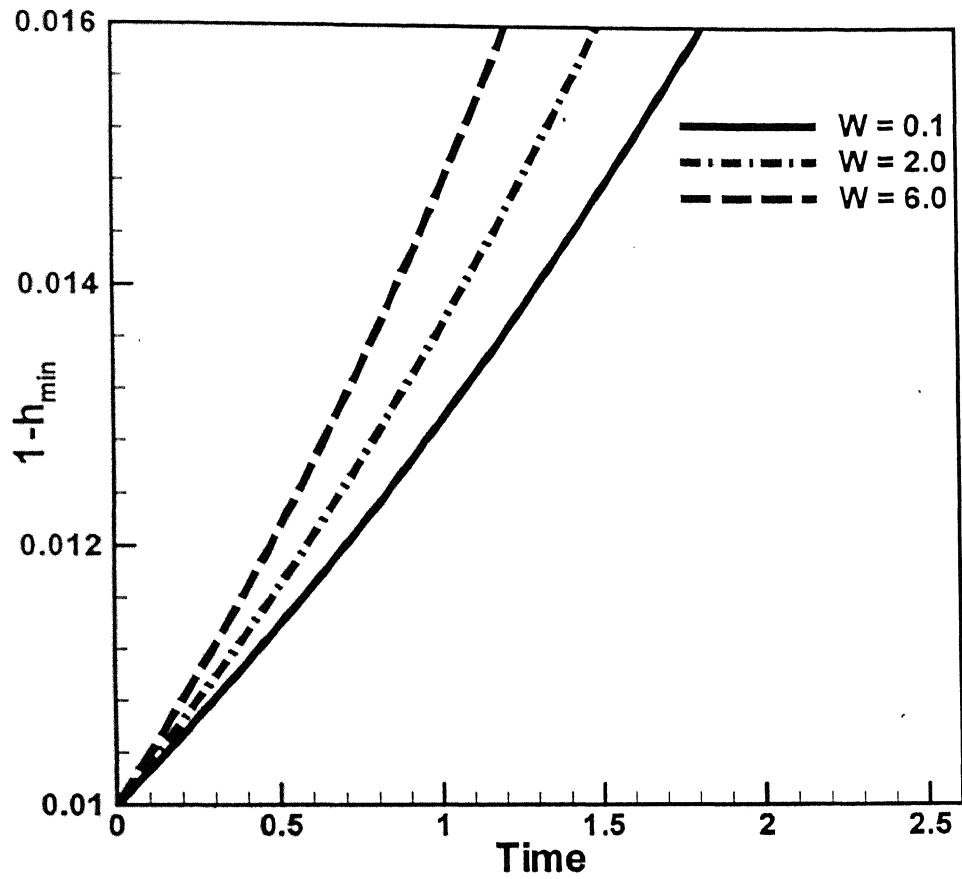


Figure 2.10. Variation of amplitude as a function of time, with weissenberg number as a parameter. As the value of weissenberg number increases the amplitude of instability increases and hence the rupture time decreases.

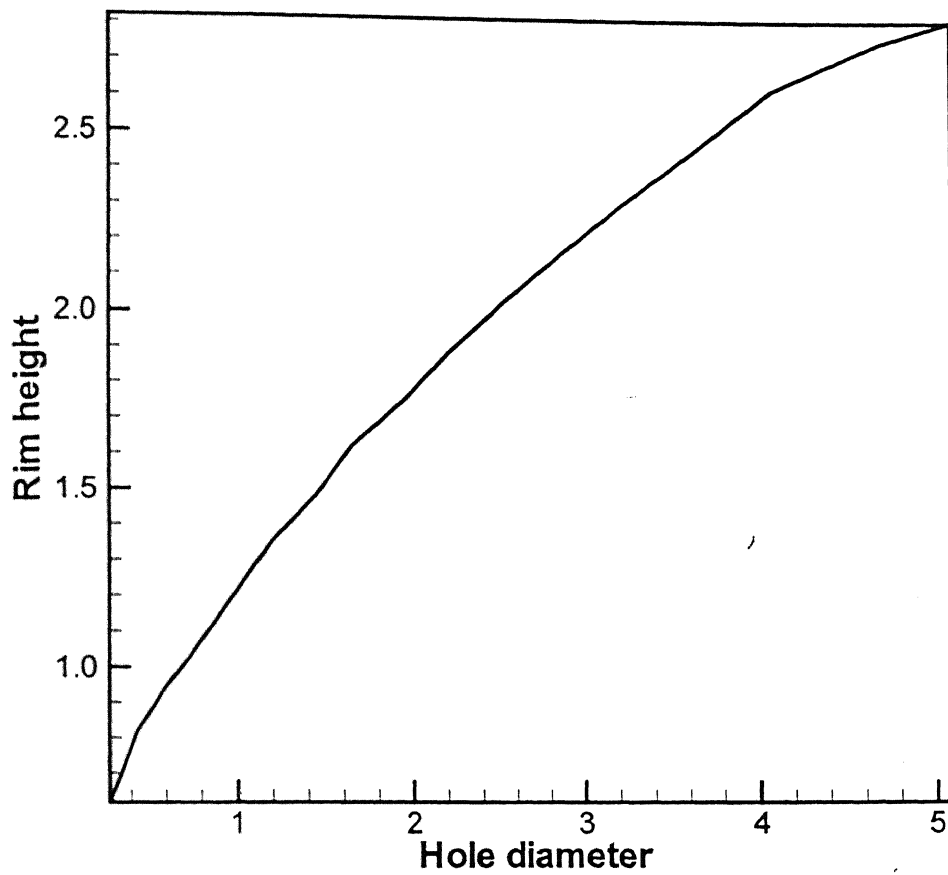


Figure 2.11 Variation between rim height as hole diameter for ($\eta_r = 0.5, w = 4.0$)

Figure 2.10 shows the variation between rim height and hole diameter that comes out to be linear in nature.

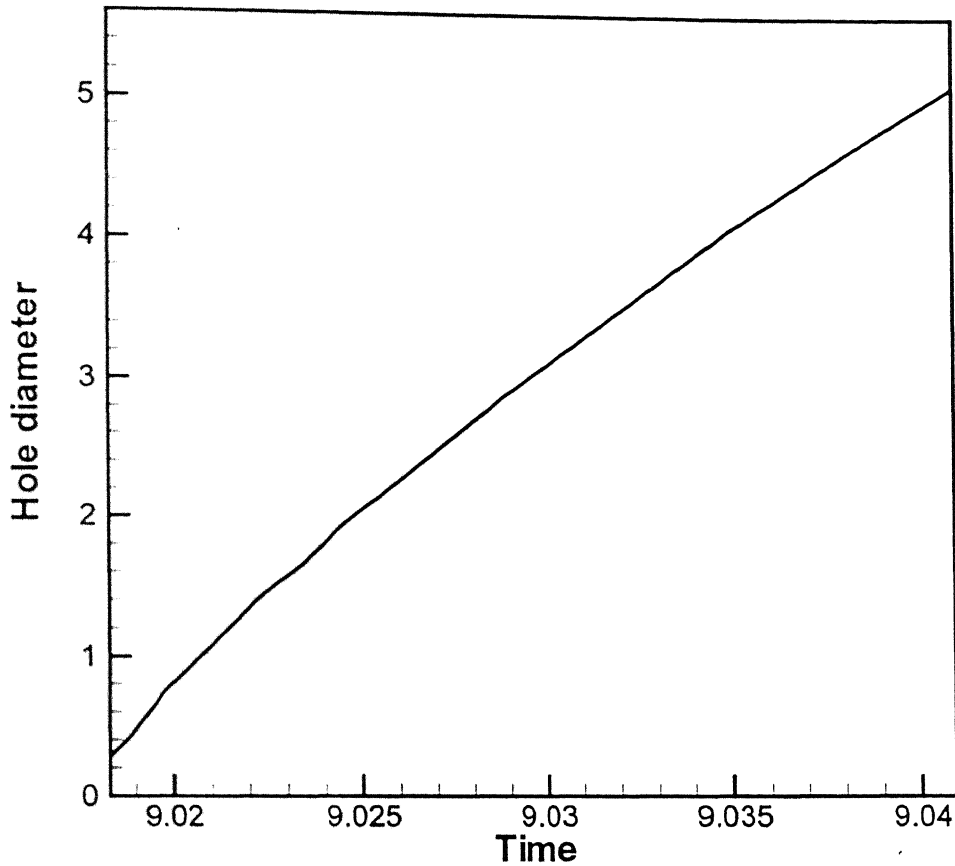


Figure 2.12 hole diameter as a function of time, for $\eta_r = 0.5, w = 4.0$

Above figure shows the variation between hole diameter as a function of time. This is linear in viscoelastic case. For Newtonian case, also it is linear.

Oldroyd B model has two limiting cases:

- Maxwell model when $\eta_r = 0$
- Newtonian case when $\eta_r = 1, w = 4.0$

2.9.4 Maxwell model

This model is the limiting case of Oldroyd B model. In this case there is no solvent but only polymer is present hence the ratio of solvent viscosity to the total viscosity is zero. i.e.

$$\eta_r = 0 \quad (2.53)$$

The constitutive relation for the Maxwell model is

$$\lambda \frac{\partial \tilde{\tau}_{xy}}{\partial t} + \tilde{\tau}_{xy} = \eta \frac{\partial V_x}{\partial y} \quad (2.54)$$

Hence, the governing equations for the Maxwell model are same but with $\eta_r = 0$ in the set of equations (2.36), (2.37) and (2.38).

In this case also the length scale of instability is $2\sqrt{2}\pi$, same as for Newtonian case. But time scale of rupture is decreased.

The maximum growth coefficient for the Maxwell model is given by taking the limit of $\eta_r = 0$ in the equation (growth coefficient).

Or

$$s_{\max} = \frac{1}{4-w} \quad \text{if } w < 4 \quad (2.55)$$

$$s_{\max} = \frac{1}{(w-4)} + \frac{2(w-4)}{8\eta_r w} \quad \text{if } w > 4 \quad (2.56)$$

Maxwell model has very interesting case when weissenberg constant approaches to 4. If ($w < 4$) then growth rate would be given by equation (above), but as weissenberg number approaches 4, growth coefficient increases rapidly. If ($w > 4$) then growth coefficient is inversely proportional to η_r , which makes it (growth coefficient) very high. It is also clear from the graph below, as the value of $w = 8$, the amplitude increases rapidly as the time increases. But for $w = 2$, it is not as fast as for the previous case.

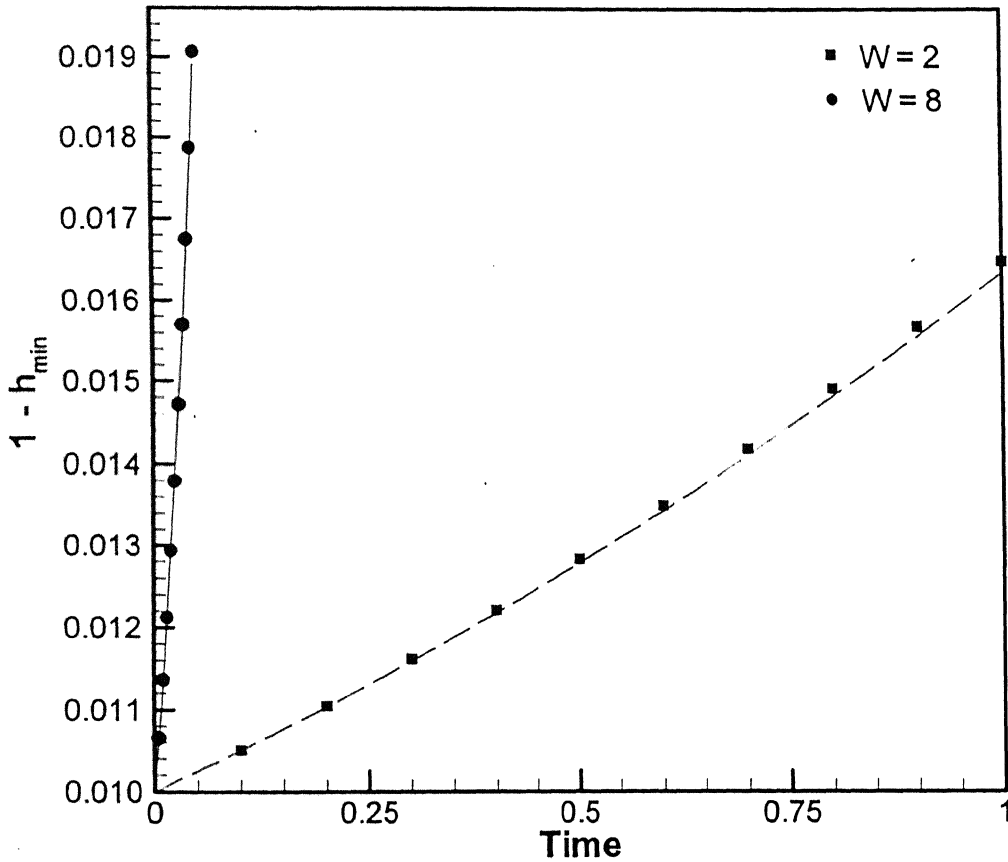


Figure 2.13. Variation of amplitude ($1 - h_{\min}$) with respect to time, for different values of weissenberg number, for very less value of η_r , ($\eta_r = 0.01$), and comparison with the

LSA. Lines are from Linear Stability Analysis and points shows the results from non-linear simulation.

Figure 2.13 shows the variation of amplitude with respect to time, with two different values of weissenberg number. One is less than 4 and other greater than 4. If $w > 4$, growth coefficient increases rapidly for very lesser value of η_r . But it is not the case when $w < 4$. For both these cases non-linear simulation results have shown a good match with the linear theory, in the initial stages of time.

2.9.5 Purely Newtonian case

In the Newtonian case, stress is linearly proportional to strain rate i.e. $\tilde{\tau}_{ij} = \eta (\partial_i V_j + \partial_j V_i)$ where, η is a constant, called, viscosity of fluid. For this case there is no polymer present in the solution. Hence, when $\eta = \eta_s$ i.e. ,

$$\eta_r = 1 \quad (2.57)$$

constitutive relationship corresponds to Newtonian fluids.

In the constitutive equation of Oldroyd B model if we put $\eta_r = 1$ then it can be simplified to,

$$\tilde{\tau}_{xy} = \eta \frac{\partial V_x}{\partial y} \quad (2.58)$$

So, Newtonian fluid is also one of the limiting cases of Oldroyd B model.

In the previous work of Ghatak A., Khanna R. and Sharma A, it is already shown that length scale of instability for Newtonian film is $2\sqrt{2}\pi$. And the maximum growth coefficient is given by, from the equation (2.34), is independent of weissenberg number.

$$s_{\max} = \frac{1}{4} \quad (2.59)$$

In the main governing equation (2.34) if η_r is replace by one and taking weissenberg number to be zero its time scale is indifferent of the work done in [15]

2.10 CONCLUSIONS AND RECOMMENDATIONS

Elasticity plays an important role in the thin film instability phenomenon. Though the length scale of instability remains same and hence elasticity has no influence on the length scale, but time scale is abruptly changes. As the elasticity or weissenberg number increases, time of rupture decreases and as the weissenberg number reaches its critical value 4 (in Maxwell Case), the growth rate increases rapidly, and hence time of rupture decreases. As the polymer is added in the solution, or ratio of solvent viscosity to the solution viscosity is decreased, rupture time is decreases, but length scale of instability is unaffected. Greater insight into the nature of problem can be obtained by carrying out a three dimensional analysis.

CHAPTER 3

EFFECT OF BENDING MOMENT IN A CELL MEMBRANE

3.1 INTRODUCTION

In the process of cell adhesion, stabilizing effect of interfacial tension and bending moment is important. Bending moment like the interfacial tension has stabilizing effect in thin films. The Bending moment becomes important where there is a significant curvature change. In the present study, simulation work is being shown for 2-D and 3-D cases, for different types of fluids sandwiched between cell membrane and solid substrates. Both the long range Lifshitz-van-der-Waal and short range Acid-Base interactions are taken in the account. The non equilibrium thin films on solid substrate either rupture completely with the appearance of three phase contact line or undergo a morphological phase separation (MPS). When the apolar (LW) and polar (P) components of the spreading coefficient are of opposite signs, thin non equilibrium films can undergo a morphological phase separation [17] Type IV films come under this category for which ($S^{LW} > 0$ and $S^{AB} < 0$)

3.2 CONCEPT OF BENDING MOMENT

Let us consider the thin fluid film sandwiched between solid substrate and cell membrane. If the layer is initially flat and it is bent then a bending moment is produced by the expansion of upper layer and compression of lower layer, followed by an area change. This bending moment is related to the local curvature and expressed as [16]

$$M = B \left(\frac{1}{R_1} + \frac{1}{R_2} \right) \quad (3.1)$$

Where, B is bending rigidity constant, and is function of the membrane properties like compressibility of the layers. Here R_1 and R_2 are local radii of curvature and force due to bending moment is obtained as $\nabla^2 M$. This is an extra term comes in pressure, so the pressure difference can be written as.

$$\Delta p = -\gamma \left(\frac{1}{R_1} + \frac{1}{R_2} \right) + B \nabla^2 \left(\frac{1}{R_1} + \frac{1}{R_2} \right) \quad (3.2)$$

Where, γ is surface tension.

3.3 Problem Formulation

Here a fluid film is considered sandwiched between a cell membrane and solid support. There are two interfaces, one at the bottom of the film, between the film and the solid substrate and the other between the film and cell membrane at the top where film touches the cell membrane.

We start with a fluid film of mean thickness h_0 and a small perturbation is given. The motion of fluid inside the film can be described by the Navier-Stokes equation, using the periodic boundary condition. Fluid is also considered to be incompressible in nature.

The evolution equation, using the long wave analysis (with condition $h_0/L \ll 1$) can be written as [13, 14].

$$h_t - \frac{1}{12\mu} \frac{\partial}{\partial x} \left[h^3 \frac{\partial}{\partial x} (p + \phi) \right] = 0 \quad (3.3)$$

Where, h is the height of free surface, p and ϕ are given by.

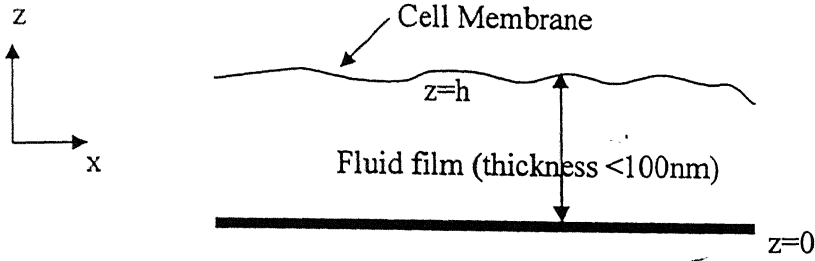


Figure 3.1 Configuration of system

$$p = -\gamma h_{xx} + B h_{xxx} \quad (3.4)$$

$$\phi = -\frac{2S^{LW}d_0^2}{h^3} - \frac{S^{AB}}{l_0} \exp\left[\frac{d_0 - h}{l_0}\right] \quad (3.5)$$

Where, S^{LW} and S^{AB} are the apolar and polar component of spreading coefficient respectively. d_0 is the cut-off distance and l_0 is the correlation length ($\cong 0.6$ nm.)

[sfe4.fig56]

3.4 Non-Dimensionalisation

The above equation can be non-dimensionalised using the parameters given below to solve for minimum number of parameters and make the equation compact.

$$H = h/h_0, d = d_0/h_0 \text{ and } l = l_0/h_0 \quad (3.6)$$

$$P = -\frac{S^{AB}}{S^{LW}(6d^2l^2)} \quad (3.7)$$

The non-dimensional space and time scaling,

$$X = ax/h_0 \text{ and } T = b\tau v/h_0^2 \quad (3.8)$$

Where

$$a = \left(\frac{6 |S^{LW}| d^2 h_0^2}{B} \right)^{1/4}, \quad b = \left(\frac{d^2 h_0 |S^{LW}| a^2}{2v^2 \rho} \right), \quad v = \mu / \rho \quad (3.9)$$

The equation after non-dimensionalisation can be written as ,

$$H_T + \left[H^3 (AH_{xx} - H_{xxxx} - \Phi) \right]_x = 0 \quad , \quad (3.10)$$

Where , A is given by,

$$A = \frac{\gamma h_0}{(6 |S^{LW}| B d^2)^{1/2}} \quad (3.11)$$

And, Nondimensional potential is given by,

$$\Phi = \text{sgn}(S^{LW}) \left[-\frac{1}{3H^3} + Pl \exp \left\{ \frac{d-H}{l} \right\} \right] \quad (3.12)$$

The dimensional equation is,

$$12\mu h_t + \left[\gamma h^3 h_{xxx} \right]_x - \left[Bh^3 h_{xxxx} \right]_x - \left[\phi h^3 h_x \right]_x = 0 \quad (3.13)$$

Equation 3.13 is the sum of four forces, per unit width of thin film, which from left to right are viscous forces, surface tension force, force due to bending moment and intermolecular force. The viscous forces merely retard the growth of instability, but

surface tension force tries to stabilize the thin film until the rupture occur after that it helps in hole growth. Bending moment term also stabilize the thin film. The intermolecular forces engender instability if $\phi_h < 0$, causing the flow from thinner region to thicker region, thus leading to dewetting.

3.5 Three-dimensional thin film equation

In the three dimensional is described by introducing the y-component in the hydrodynamic equation. The evolution equation in three dimensional is

$$12\mu h_t + \left[h^3 \left\{ \gamma (h_{xx} + h_{yy}) - B(h_{xxx} + h_{yyy}) - \phi \right\}_x \right]_x + \left[h^3 \left\{ \gamma (h_{xx} + h_{yy}) - B(h_{xxx} + h_{yyy}) - \phi \right\}_y \right]_y = 0 \quad (3.14)$$

The three dimensional Nondimensional evolution equation is,

$$H_t + \left[H^3 \left\{ A(H_{xx} + H_{yy}) - H_{xxx} - H_{yyy} - \Phi \right\}_x \right]_x + \left[H^3 \left\{ A(H_{xx} + H_{yy}) - H_{xxx} - H_{yyy} - \Phi \right\}_y \right]_y = 0 \quad (3.15)$$

3.6 LINEAR STABILITY ANALYSIS

Linear stability analysis predicts the initial growth of thin films by linearizing the height around $H = 1$. The linear equation admits solution of the form

$$h = h_0 + \varepsilon \exp(ikx + \omega t) \quad (3.16)$$

Where ε is the ratio of initial amplitude of perturbation to mean film thickness.

The equation can also be linearized in Nondimensional form as,

$$H = 1 + E \exp(iKX + \Omega T) \quad (3.17)$$

Where E is the initial perturbation, K is the Nondimensional wave number and Ω is Non-dimensional growth coefficient. The linear dispersion relation relating the growth coefficient to the wave number can be written as,

$$\omega = \left(-h_0^3 / 12\mu \right) \left[\gamma k^4 + Bk^6 + (\phi_h)_{h=h_0} k^2 \right] \quad (3.18)$$

It can also be expressed in the Nondimensional form as

$$\Omega = -K^2 \left[AK^2 + K^4 + (\Phi_H)_{H=1} \right] \quad (3.19)$$

i.e.

$$\Omega = -AK^4 - K^6 - \text{sgn}(S^{LW}) \left[1 - P \exp \left\{ \frac{d-1}{l} \right\} \right] K^2 \quad (3.20)$$

Growth coefficient will increase as the wave number is increased. It reaches a maximum and then starts decreasing, so the dominant wave number is defined as k_m , for which growth coefficient ω is maximum, or $\frac{\partial \omega}{\partial k} = 0$.

$$k_m = \sqrt{\frac{-\gamma + \sqrt{\gamma^2 - 3B(\phi_h)_{h=h_0}}}{3B}} \quad (3.21)$$

The critical wavelength is defined the wave number at which growth coefficient vanishes i.e. $\omega = 0$.

$$k_c = \sqrt{\frac{-\gamma + \sqrt{\gamma^2 - 4B(\phi_h)_{h=h_0}}}{2B}} \quad (3.22)$$

i.e. for the wave length greater than the critical wavelength, all perturbation will die out

and $h = h_0$ will be the steady state solution.

In the Nondimensional form it can be written as,

$$K_m = \sqrt{\frac{-A + \sqrt{A^2 - 3(\Phi_H)_{H=1}}}{3}} \quad (3.23)$$

$$K_c = \sqrt{\frac{-A + \sqrt{A^2 - 4(\Phi_H)_{H=1}}}{2}} \quad (3.24)$$

There are two asymptotic cases.

1) $B \rightarrow 0$

$$k_{m\gamma} = \left[\frac{-(\phi_h)_{h=h_0}}{2\gamma} \right]^{1/2} \quad (3.25)$$

2) $\gamma \rightarrow 0$

$$k_{mB} = \left[\frac{-(\phi_h)_{h=h_0}}{3B} \right]^{1/4} \quad (3.26)$$

The dominant wave length Λ_m is related to the dominant wave number by the relation,

$$\Lambda_m = 2\pi / K_m \quad (3.27)$$

The time of rupture can also be predicted by the linear theory, by putting $H=0$ and $\cos(KX) = -1$ in equation (3.17). This gives the time of rupture, i.e. the time at which first time film surface touches the solid substrate, in terms of initial perturbation amplitude and maximum growth coefficient.

$$T_R = \frac{1}{\Omega} \ln \left[\frac{1}{E} \right] \quad (3.28)$$

3.7 Numerical Method (2D)

The non-linear equations, derived earlier are sixth order nonlinear partial differential equation in space. It is discretized using central differential technique using half node interpolation. The resulting set of ODEs are very stiff in nature because the wide disparity between length scale and time scale. Hence this initial value problem is solved using Gear's technique which is appropriate for stiff set of differential equations. Nag library subroutine D02EJF which employs Gear's algorithm is used to integrate the ODEs Equation (3.10) is solved in an X domain using the periodic boundary condition. This length is divided in to N parts using the finite difference hence this PDE is being converted in to N number of ODEs, each node represents an ODE.

$$\Delta X = L / (N - 1) = \Delta$$

We can reach at i^{th} node by

$$X_i = (i-1)\Delta \quad (3.29)$$

If the film thickness at the i^{th} node is H_i then derivative at this point is given by

$$\frac{dH_i}{dT} = \frac{F1_{i+1/2} - F1_{i-1/2}}{\Delta} \quad (3.30)$$

Where,

$$F1_i = \left[H^3 (-AH_{,XX} + H_{,XXX} + \Phi) \right]_{,X} \Big|_i = H_i^3 \frac{F2_{i+1/2} - F2_{i-1/2}}{\Delta} \quad (3.31)$$

$$F2_i = [-AH_{,XX} + H_{,XXX} + \Phi]_i$$

Where, this spatial derivatives are further discretized using the central difference technique, given below.

$$[H_{xx}]_i = \frac{H_{i+1} - 2H_i + H_{i-1}}{\Delta^2} \quad (3.32)$$

And

$$[H_{xxxx}]_i = \frac{H_{i+2} - 4H_{i+1} + 6H_i - 4H_{i-1} + H_{i-2}}{\Delta^4} \quad (3.33)$$

3.8 Numerical Method (3D)

The three dimensional equation is solved in L^2 domain using the periodic boundary condition. The equation is discretized using the central difference technique using the half node interpolation. Because the equation is very stiff in nature hence D02NCF routine from the Nag library, which employs Gear's algorithm, is used to solve the N^2 number of differential equation. Fluid surface is parallel to the X-Y plane and Z direction is normal to the film. Finite difference technique, taking both the difference in X and Y direction same, has been used.

$$\Delta X = \Delta Y = L/(N-1)$$

To reach at any location at (X_i, Y_j) we can simply write

$$(X_i, Y_j) = ((i-1)\Delta, (j-1)\Delta) \quad (3.34)$$

If the film thickness at the (X_i, Y_j) location is H_{ij} then the derivative at this point can be written as,

$$\frac{dH_{ij}}{dT} = \frac{FlX_{i+1/2,j} - FlX_{i-1/2,j}}{\Delta} + \frac{FlY_{i,j+1/2} - FlY_{i,j-1/2}}{\Delta} \quad i,j = 1,2,3,\dots,N \quad (3.35)$$

Where function FlX is given by,

$$F1X_{i,j} = \left[H^3 \left\{ -A(H_{xx} + H_{yy}) + H_{xxx} + H_{yyy} + \Phi \right\}_x \right]_{i,j} = H_{i,j}^3 \frac{F2_{i+1/2,j} - F2_{i-1/2,j}}{\Delta} \quad (3.36)$$

Similarly the function F1Y is given by,

$$F1Y_{i,j} = \left[H^3 \left\{ -A(H_{xx} + H_{yy}) + H_{xxx} + H_{yyy} + \Phi \right\}_y \right]_{i,j} = H_{i,j}^3 \frac{F2_{i,j+1/2} - F2_{i,j-1/2}}{\Delta} \quad (3.37)$$

Where F2_{i,j} is given by,

$$F2_{i,j} = \left\{ -A(H_{xx} + H_{yy}) + H_{xxx} + H_{yyy} + \Phi \right\}_{i,j} \quad (3.38)$$

Discretization in space is done, using central difference technique in space. the whole domain is divided in to N x N number of points. Now at each point the partial differential equation converts to an ordinary difference equation. hence this PDE in the whole domain converts to the N² number of ODEs. Nag library subroutine D02NCF is used to solve these N² number of ordinary differential equations. This subroutine employs Gear's technique which is best suited for the stiff differential equations. The 60 X 60 points were found to be sufficient for the grid convergence test.

3.9 RESULTS AND DISCUSSION

The total spreading coefficient can be calculated using the equations below for LW and Acid-Base components, for the system described above.

$$S^{LW} = 2 \left[\sqrt{\gamma_c^{LW}} - \sqrt{\gamma_f^{LW}} \right] \left[\sqrt{\gamma_f^{LW}} - \sqrt{\gamma_s^{LW}} \right] \quad (3.39)$$

$$S^{AB} = 2 \left[\sqrt{\gamma_f^+} \left(\sqrt{\gamma_c^-} + \sqrt{\gamma_s^-} - \sqrt{\gamma_f^-} \right) + \sqrt{\gamma_f^-} \left(\sqrt{\gamma_c^+} + \sqrt{\gamma_s^+} - \sqrt{\gamma_f^+} \right) - \sqrt{\gamma_c^- \gamma_s^+} - \sqrt{\gamma_c^+ \gamma_s^-} \right] \quad (3.40)$$

Where, subscript c, f, s are corresponding to the cell membrane, fluid film and the substrate. S^{LW} and S^{AB} are spreading coefficients for Lifshitz–vander Waals and Acid-Base components, respectively. The typical value of bending moment is taken to be 10^{-13} ergs [7] for all the cases.

The relative importance of bending moment is clear if the dominant length scale of the case bending moment with no interfacial tension is compared with only interfacial tension case.

The dominant length scale for the case with bending moment and no interfacial tension is given by,

$$\lambda_{mB} = 2\pi \left[\frac{3B}{-(\phi_h)_{h=h_0}} \right]^{1/4} \quad (3.41)$$

Similarly, the dominant length scale for the case with interfacial tension with no bending moment is given by,

$$\lambda_{m\gamma} = 2\pi \left[\frac{2\gamma}{-(\phi_h)_{h=h_0}} \right]^{1/2} \quad (3.42)$$

The ratio $R_{\lambda m} = \lambda_{mB} / \lambda_{m\gamma}$ can be written as,

$$R_{\lambda m} = \left(\frac{3B(-\phi_h)_{h=h_0}}{4\gamma^2} \right)^{1/4} \quad (3.43)$$

It is clear from equation (3.26) that for low values of surface tension, the effect of bending moment has to be considered, otherwise length scale of instability will be very

low and hence long wave analysis will not be applicable in this case. Lastly, for higher value of h_0 and γ , the effect of bending moment can be neglected eq. (3.18). The bending moment stabilizes the system as it is evident from figure (3.2) which shows the inverse relation of growth coefficient with the bending moment.

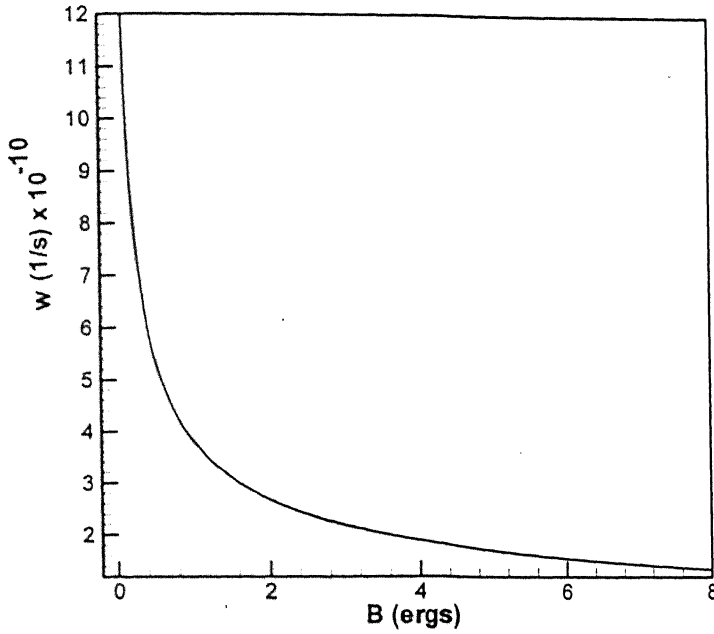


Fig. 3.2 Variation of growth coefficient with the bending moment.

To analyze the system, it has been dividend in to two main parts. First is the case when the Acid-Base interaction vanishes, i.e. ($S^{AB} = 0$) and hence ($P = 0$). The second part is

when ($P \neq 0$), this part is further subdivided into two parts. The first sub-case is when the substrate is apolar and in other sub-case substrate is polar.

CASE 1: $P = 0$

In this case, the fluid film and any one of, either the substrate or the cell membrane is apolar in nature. For this case the Acid-Base component of the Spreading coefficient vanishes, i.e. $S^{AB} = 0$, it is also self exemplified from the equation (3.40). Hydrocarbon film in contact with the lymphocyte cell is one of the examples. S^{LW} component should be taken to be negative to describe the attractive behavior of Lifshitz-vander Wall component.

For this case from the equations (3.12) and (3.23), it is clear that dominant wave number has inverse dependence on A , a function of γ and h_0 . The behavior for this case is of Type I system, where ϕ_h is negative for all film thicknesses. It is observed from the non-linear simulations that for any value of B , the system will be destabilized from the effect of attracting (destabilizing) Lifshitz-vander Wall component [10].

Case: 2 ($P \neq 0$)

In this case, both the polar and apolar interactions are taken into account. This system is further divided into two parts, in the first one apolar substrate is taken and in the second one polar substrate is taken. In both the cases, cell membrane is taken to be polar in nature. In the first case, when the substrate is apolar, the system is chosen in such a way that S^{LW} component is positive i.e. from the equation (3.39) it is clear that for S^{LW} to be positive (stabilizing), the Lifshitz-vander Wall component of the free energy of the film should lie in between the LW component of free energy of substrate and the cell

membrane. i.e. $\gamma_c^{LW} > \gamma_f^{LW} > \gamma_s^{LW}$ or $\gamma_c^{LW} < \gamma_f^{LW} < \gamma_s^{LW}$, and S^{AB} component of free energy to be negative (destabilizing). In the second case substrate is chosen in such a way that S^{LW} component is negative and S^{AB} component is positive. The above two cases comes in the category of Type II system and Type IV systems.

Type II Systems

Type II systems are a combination of long wave repulsion and short wave attraction. S^{LW} , which is long range force, is negative while S^{AB} , which is short range Acid-Base force, is positive.

Type IV Systems

Type IV systems are a combination of negative, long range attraction of Lifshitz–vander Wall forces and positive, short range repulsion of Acid-Base forces. The graphs for these two systems are shown below.

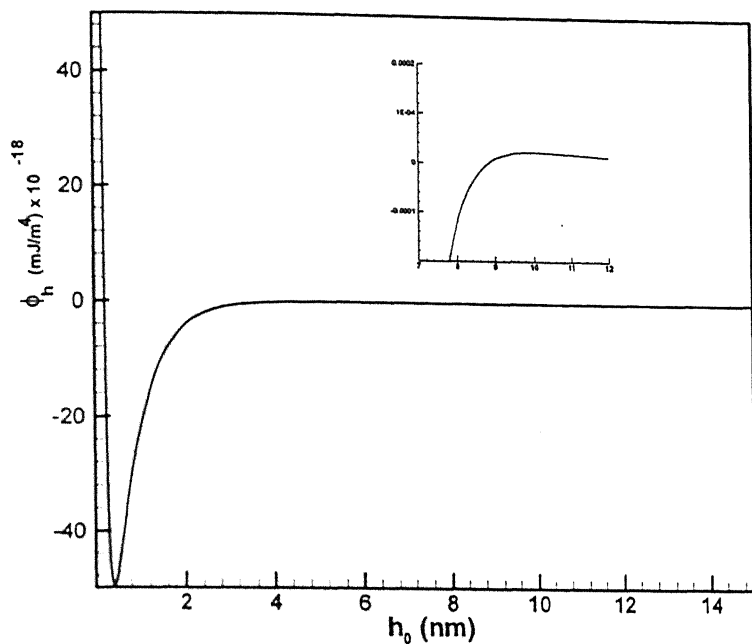


Fig 3.3. Variation of ϕ_h with the mean film thickness for Type IV systems. S^{LW} is 2.0 mJ/m² and S^{AB} is -33.0 mJ/m².

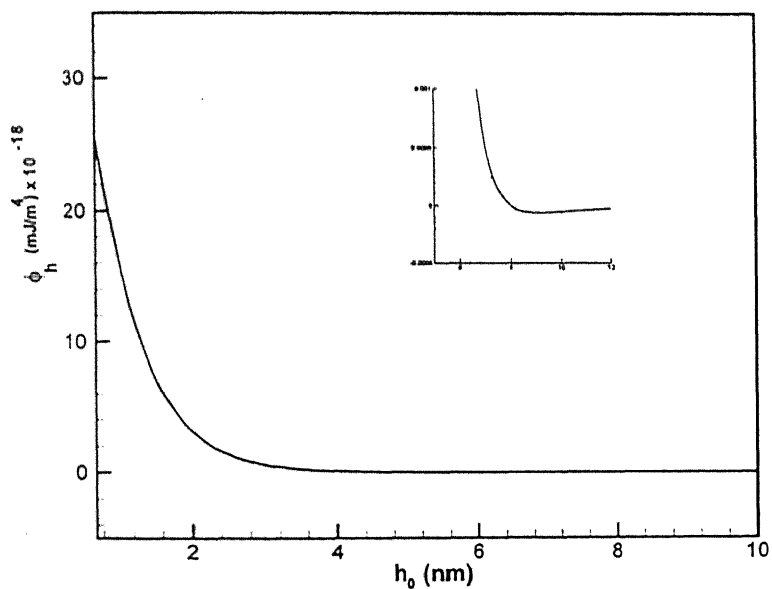


Fig 3.4. Variation of ϕ_h with the mean film thickness for Type IV systems. $S^{LW} = -4.0$ mJ/m² and $S^{AB} = 25.0$ mJ/m².

Apolar Substrate

Figure 3.5 shows the profile of thin film in 2-D case, in 2Λ length scale where Λ is the dominant wave length corresponding to that film thickness, with mean thickness as the parameter. As the initial mean film thickness is increased, there is the increase in the peak value. The Nondimensional time of rupture is increased as the mean thickness is increased, which indicate that film rupture is faster in thinner films.

Figure 3.6 shows the effect of interfacial tension at constant mean film thickness. It shows that as the value of interfacial tension is increased there is an increase in the rupture time; this is because surface tension has stabilizing influence.

Figure 3.7 shows the whole morphology of thin sinusoidal film, with mean thickness $h_0 = 5$ nm and initial perturbation of ϵ , on a length scale of 2Λ , where Λ is the dominant length scale. Because of the negative value of ϕ_h which signifies, higher pressure in thinner region and lower pressure in thicker region. Hence the flow starts from thinner region to thicker region leading to the film stability. The amplitude of wave start growing and at one point the film surface touches the surface and making hole which starts growing with time. Simultaneously a rim starts growing near the hole, which also increases as the time increases. Finally two neighboring rims start interacting and make a bigger drop.

In Fig 3.8, length scale of 3Λ is taken for the simulation, where Λ is the dominant length scale given by linear stability analysis. A thin film of mean thickness of 5.0 nm and initial amplitude of random perturbation of ($\epsilon=0.01$) was taken for the simulation. Three waves start forming on this length scale which validates the simulation.

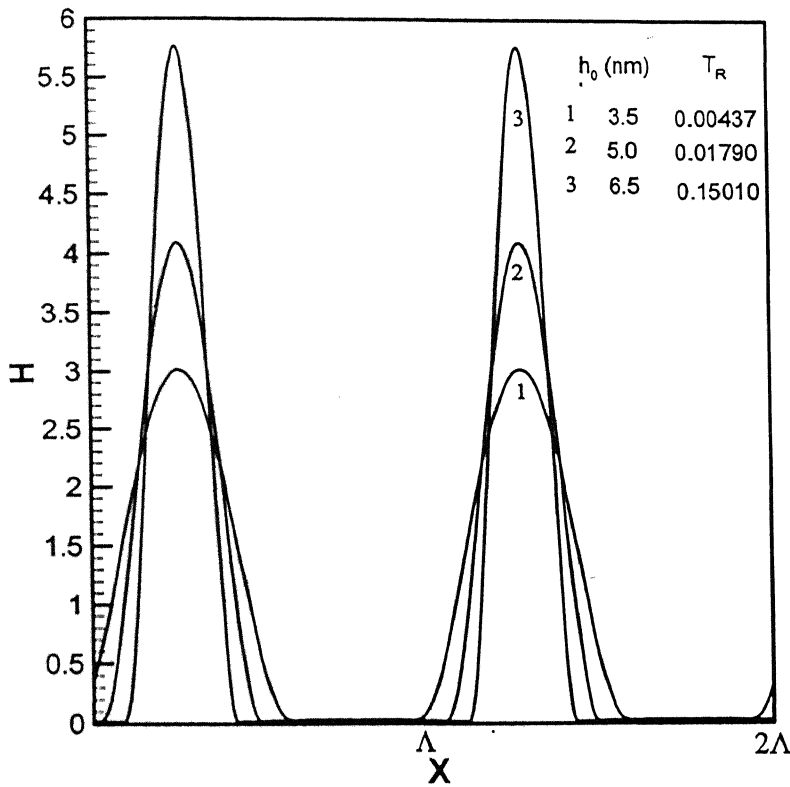


Figure 3.5. Final profile of the thin film, with mean height as the parameter, starting with sinusoidal perturbation, for apolar substrate, $S^{LW} = 2.0 \text{ mJ/m}^2$ and $S^{AB} = -33.0 \text{ mJ/m}^2$. Surface tension $\gamma = 0.001 \text{ mJ/m}^2$.

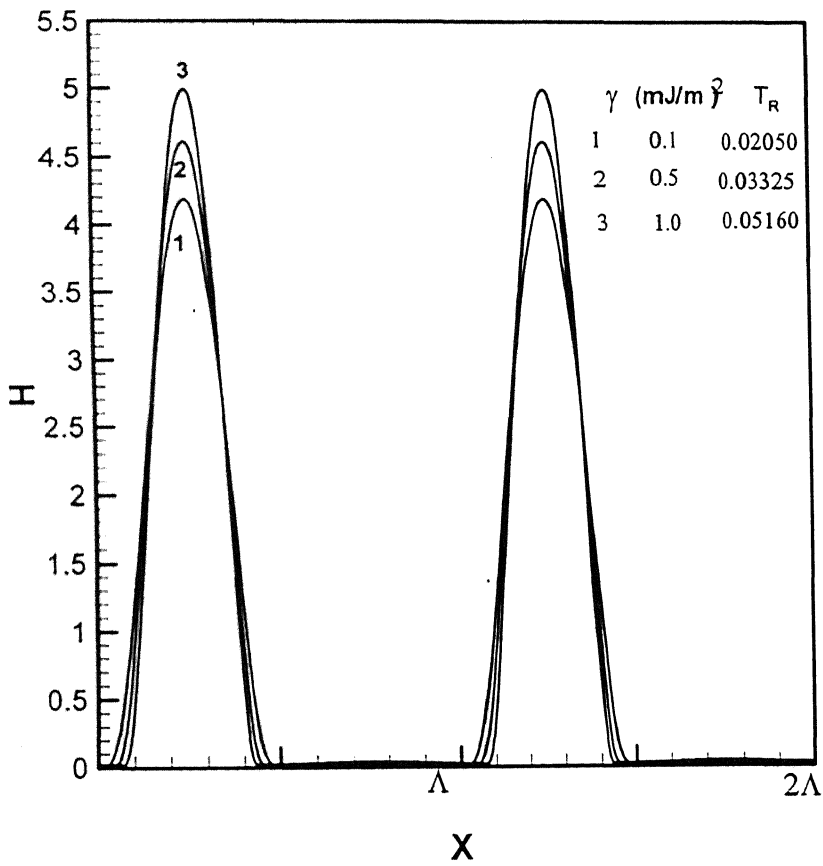


Figure 3.6 Final profile of the thin film, with surface tension as the parameter, starting with sinusoidal perturbation, for apolar substrate, $S^{LW} = 2.0$ mJ/m² and $S^{AB} = -33.0$ mJ/m². Mean height $h_0 = 5$ nm.

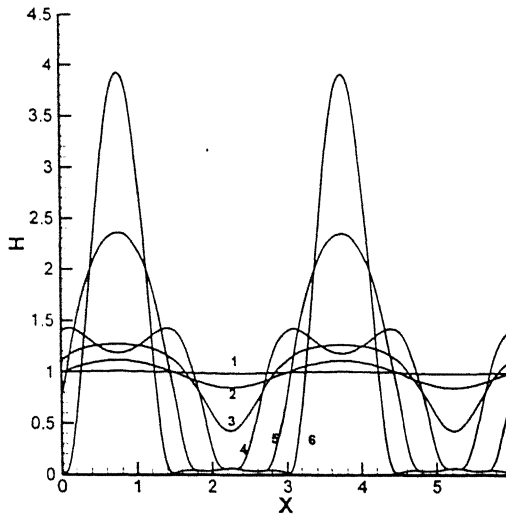


Figure 3.7 Full morphology of thin film starting with mean film thickness $h_0 = 5$ nm. On 2Λ length scale, for apolar substrate $S^{LW} = 2.0$ mJ/m², $S^{AB} = -33.0$ mJ/m². Surface tension $\gamma = 0.001$ mJ/m².

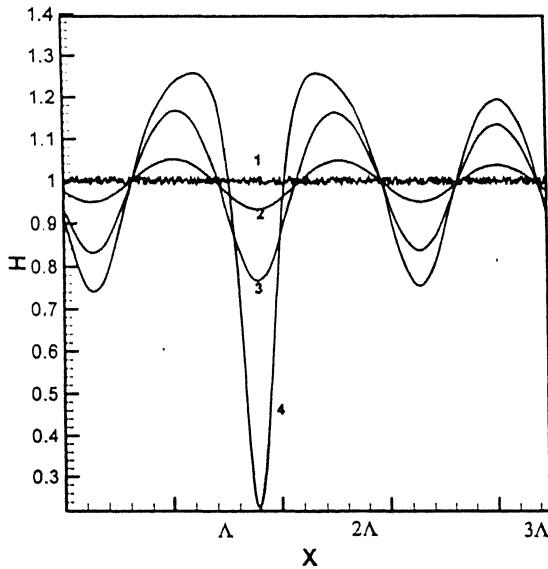


Fig 3.8. Morphology of thin film starting with mean film thickness $h_0 = 5$ nm and with random perturbation of $\varepsilon = 0.01$. On 3Λ length scale, for apolar substrate $S^{LW} = 2.0$ mJ/m², $S^{AB} = -33.0$ mJ/m². Surface tension $\gamma = 0.001$ mJ/m².

Polar Substrate

In this case substrate is taken to be apolar in nature. The values of spreading coefficients are taken such that this system behaves like a Type II system i.e. S^{LW} is negative and S^{AB} is positive. Again the sign of both the spreading coefficients are negative, we expect Morphological Phase Separation (MPS) i.e. formation of a stable interconnected microstructure consisting of an array of small drops in equilibrium with the thin films. Figure 3.9 shows the final profiles of thin films on polar substrate on 2Λ length scale starting with a sinusoidal initial perturbation, taking mean height as the parameter. As the mean height is increased, rupture time as well as the peak height increases.

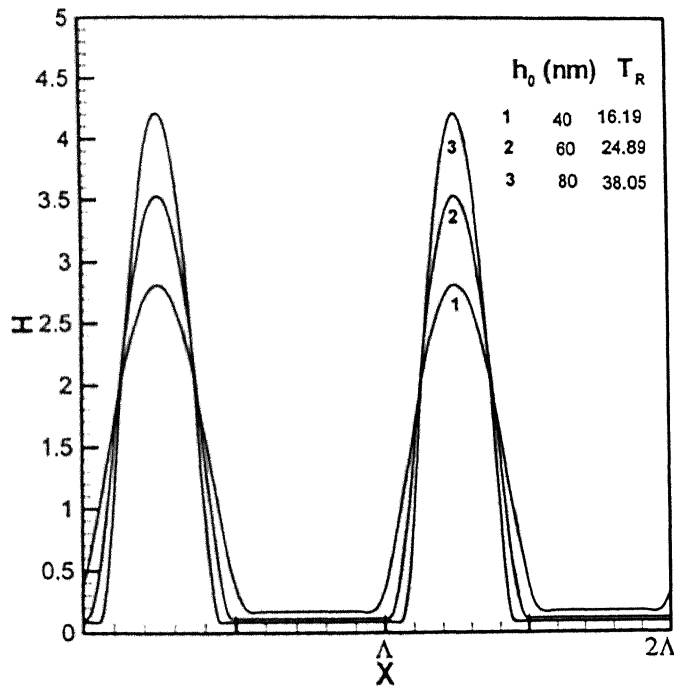


Figure 3.9. Profiles of thin films on an apolar substrate, varying mean height as the parameter. $S^{LW} = -4.0 \text{ mJ/m}^2$ and $S^{AB} = 25.0 \text{ mJ/m}^2$.

Figure 3.10 shows the 3-D simulation results for 5 nm thick film on a homogenous substrate. The length scale of instability is recognized by the linear stability analysis. It was found that two different morphological patterns and their sequence of evolution by which dewetting can occur, depends on the form of the potential in the neighborhood of the initial film thickness. Figure 3.11 summarizes the major events in the time evolution of pattern in a relatively thick 80 nm film, which is far more than the height at which ϕ_h shows minimum. The initial random disturbance is first reorganized into a small amplitude bi-continuous pattern on a length scale close to Λ . Long “hills” of the structure undergo some fragmentation, while the “valleys” thin locally to produce largely circular holes surrounded by circular uneven (in height) rims. The general pathway of evolution, whenever the initial mean thickness is sufficiently high so that the repulsive interactions at the minimum thickness are encountered only after a considerable growth of instability, can be summarized as (bi-continuous pattern \rightarrow circular holes with rims \rightarrow hole expansion \rightarrow hole coalescence) [8]. At the later stages of time it shows the breaking of rims and formation of some ridges like pattern, this instability is called Rayleigh Instability. The dewetting occurs by expansion of holes.

In contrast to the above scenario, figure 3.12 depicts a different pathway of evolution for the relatively thin films which encounter repulsion in the early stages of growth. A bi-continuous structure composed of long hills and valleys persists until the fragmentation of “hills” producing an array of microdroplets. These droplets become increasingly circular due to surface tension and increase in height due to flow from “valleys” which thins and flatten out. The droplets are circular due to the surface tension force. In this case, the dewetting occurs by the retraction of droplets, rather than by expansion of holes.

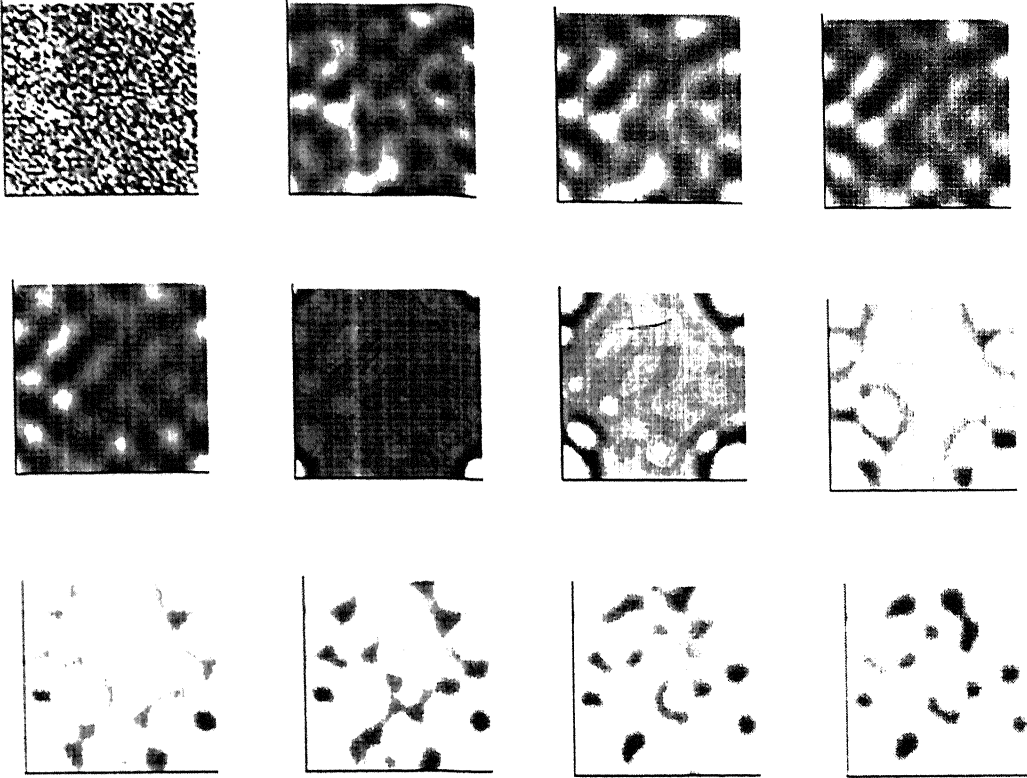


Figure 3.10 Different stages of evolution in 5.0 nm thick film, starting with random perturbation, $l_0 = 0.6$ nm, $SLW = 2$ mJ/m² and $S^{AB} = -33.0$ mJ/m² the area of each box is $16\Lambda^2$ ($\Lambda = 2.98$, is the dominant length scale) the images correspond to from left to right at time $T = 0, 0.0016, 0.0060, 0.0130, 0.0180, 0.0215, 0.0225, 0.0228, 0.0236, 0.0240, 0.0248, 0.0277$ respectively. Increasing shades indicates increase in height.

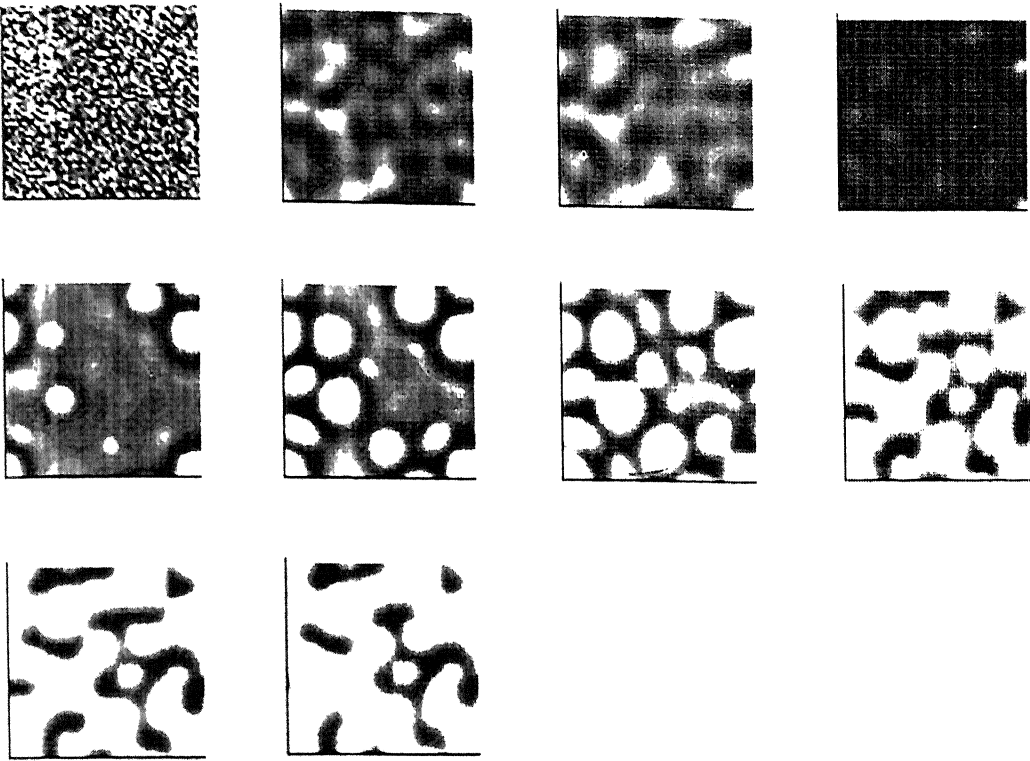


Figure 3.11. Different stages of evolution in 80 nm thick film, starting with random perturbation, $l_0 = 1.0$ nm, $SLW = -4$ mJ/m² and $S^{AB} = 25.0$ mJ/m² the area of each box is $16\Lambda^2$. The images correspond to from left to right at time $T = 0, 1.08, 14.32, 53.39, 59.51, 63.02, 66.06, 71.86, 76.99, 95.20$ respectively. Increasing shades indicates increase in height.

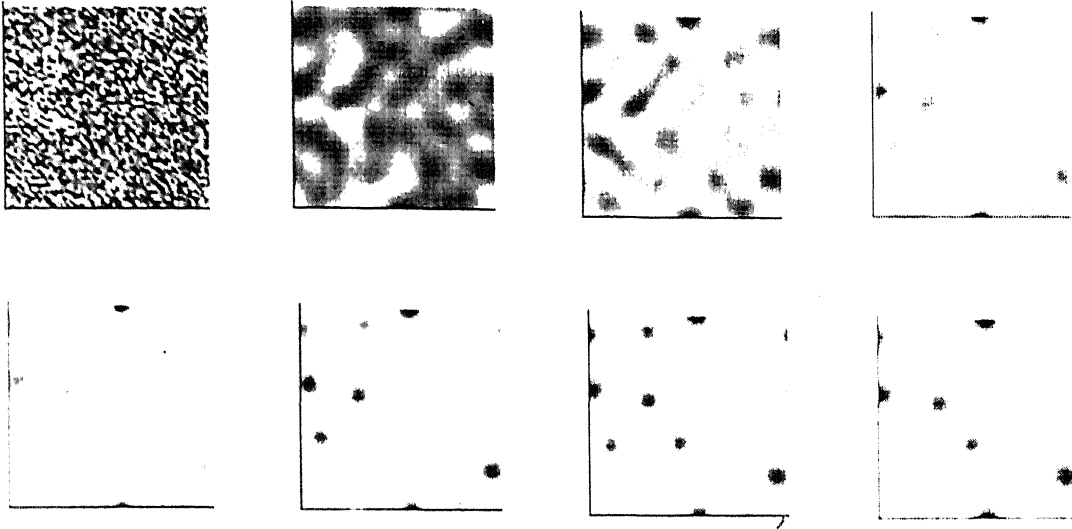


Figure 3.12 Different stages of evolution in 3.5 nm thick film, starting with random perturbation, $l_0 = 2.5$ nm, $SLW = 4$ mJ/m² and $S^{AB} = -0.1$ mJ/m² the area of each box is $16\Lambda^2$ the images correspond to from left to right at time $T = 0, 128.46, 472.07, 587.67, 629.12, 718.35, 940.31, 1811.97$ respectively. Increasing shades indicates increase in height.

3.10 CONCLUSIONS AND RECOMMENDATIONS

Bending moment plays an important and dominant role in the thin film instability. It plays an important role when surface tension has very low value. Length scale and time scale is changed, while the time scale has not been affected much by the inclusion of the bending moment because this instability is a micro drop phenomenon, but length scale is changed largely. The 3-D figures show that different initial height shows the different patterns and different phenomenon of dewetting, depending upon after what depth it feels the repulsive forces.